A Precision Manipulation System for Polymer Microdevice Production

By

Nadège Zarrouati
Ingénieur de l'Ecole Polytechnique (2008)

Submitted to the Department of Mechanical Engineering
in Partial Fulfillment of the Requirements for the Degree of

Master of Science in Mechanical Engineering

at the

Massachusetts Institute of Technology

June 2010

Author: _____
Department of Mechanical Engineering
January 10, 2010

Certified by: _____
Brian W. Anthony
Lecturer in Mechanical Engineering
Thesis Supervisor

Accepted by: _____
David E. Hardt
Professor of Mechanical Engineering
Chairman, Committee on Graduate Students

A Precision Manipulation System for Polymer Microdevice Production

Nadège Zarrouati

Submitted to the Department of Mechanical Engineering
in June 2010, in partial fulfillment of the requirements for the degree of
Masters of Science in Mechanical Engineering

Abstract

Microfluidic science is currently going through a transition from the research laboratories to the industry as the applications and technologies increase and improve. One of the challenges of this transition is the automated production of microfluidic devices for competitive costs and production rates. The objective of this thesis was to design and achieve a fully automated production of polymer-based microfluidic devices. The manipulation must be adapted to all the processing stations and its position repeatability must be within a couple of tens of microns. Based on overall consistency and modularity criterions, we selected a SCARA robot associated with a custom vacuum chuck end effector. The position repeatability was improved by an alignment strategy based on a compliant kinematic coupling. For an ideal part, this strategy divides the position uncertainty of the manipulator by a factor of 5. A model of the flow of materials in the production cell has been optimized to maximize the production rate: the shortest value of the Takt time reaches 280s.

Thesis Supervisor: Brian W. Anthony
Title: Lecturer in Mechanical Engineering

Table of Contents

List of Figures

List of Tables

Acknowledgments

I would like to thank my advisor Dr. Brian W. Anthony for his guidance and the attention he has paid to the small details that made research a pleasure for me during these two years at MIT.

I would also like to thank Pr. David E. Hardt for the advice and experience he shared during the μFAC meetings.

I would like to thank the Singapore-MIT Alliance whose funding made this project possible.

I would like to thank my labmates and the other students I worked with for their patience and their help: a special thought to Melinda who taught me so much, to Sivesh for his very competent help and to Michelle for her watchful reading of this thesis.

I would like to thank the staff of the machine shop, especially William Buckley who made sure that I could come back to France with all my fingers. A special thank to Rachel Russell and David Rodriguera for their help in any situation.

I am deeply thankful to my friends for all the good memories that we shared, and to my parents for their unconditional support.

Matthieu, thank you for always being there for me.

Chapter 1.

Introduction

The objective of this thesis is to design and achieve a fully automated production of polymer-based microfluidic devices within the Microfactory Project, known as *μFAC*. Microfluidic science is currently going through a transition from the research laboratories to the industry as the applications and technologies increase and improve. The production of microfluidic devices in clean rooms as it has been done in the last few years is long, expensive and requires trained and qualified operators. The automation of this production makes sense if the consequent cost and production rate significantly improve. In the same perspective, making the devices out of polymers is justified by its low material cost and disposability.

The *μFAC* project started in 2008 and is currently ongoing in its second version. The work presented in this thesis represents only a portion of the larger *μFAC* project, but to understand the challenges and achievements of this thesis, a quick review of the initial project is necessary (section 1.1). In the next section, the novelties of the second project relevant to this thesis and the author's specific objectives are presented.

1.1 Background: description of the initial Microfactory Project.

During the summer of 2008, a team of more than 10 research students and 4 faculty members in collaboration with the Singapore-MIT Alliance were involved in the Microfactory project, or *μFAC*. The purpose of this research project was to use and synthesize the individual knowledge of each of the members to design and test a manufacturing assembly line and produce polymer-based microfluidic devices in volumes of at least 100 units with a target Takt time of 5 minutes. A paper describes the inception of this factory [1] and the first results, and more detailed and specific results appear in papers such as [2-3] on deformation properties of polymers, [4,5,6] on novel machine and process design for hot micro embossing and PDMS Casting, [7-9] on tooling production and de-molding analysis, [10] on bonding methods and [11-14] on methods for measurement and control of the resulting processes.

The following describes in more detail the basis of the initial project that has been maintained for the *μFAC II*.

1.1.1 The product

The project was focused on the use of hot micro-embossing (HME) with polymethylmethacrilate (PMMA) as the device material. A companion production cell using a PDMS casting process was also developed, based on rapid degassing and curing. This work is currently ongoing [15].

The product of this production cell is a simple binary micro mixer. The channels are 40 microns deep and 50 microns wide. This design was chosen for numerous reasons: the dimensions of the channels make the necessary tooling easy to produce and are in the mid-range of typical microfluidic device dimensions; the resulting pressures and flow rates are reasonable and the functional testing is conceptually simple. The overall size of the product is 35 mm by 25 mm, as shown in figure 1.1.

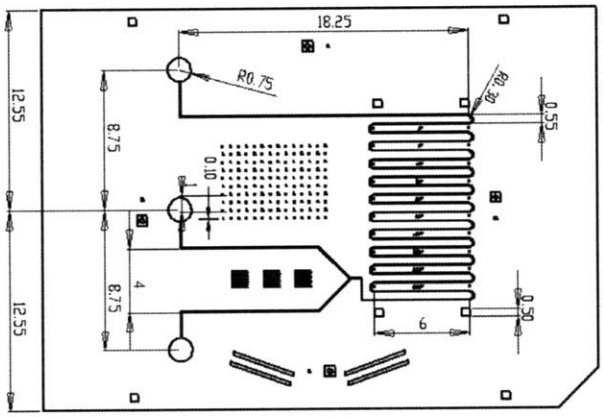

Figure 1.1: Pattern Drawing for the Micro Mixer Tooling
Showing Numerous Fiducials and Registration Features

In addition to the functional channels, the pattern also includes various fiducials, vernier scales and registration marks. These were added to help to measure the dimensions of the channels as well as the overall distortion of the substrate in the final product. The edge in the bottom right corner of the substrate is used to orientate the substrate at each step. The inlet and output ports are pre-drilled prior to embossing.

1.1.2 Production steps of the Fluid Mixer

The operations to produce the final Micro Mixer are as follows:

- The substrate blank is cut from a 1.5mm thick PMMA sheet using an Epilog MiniHelix 8000 laser cutting machine. The substrate blank consists of an overall rectangular part with 3 holes and an edge, plus an engraved serial number. Another

square substrate (25 mm by 25 mm) is also cut in the same material and will be the coverplate.

- The blank is positioned and registered in the hot micro machine (HME). The HME cycle is executed.
- The part is positioned and registered in the inspection stage, and inspected. During this geometric verification, key dimensions are measured to match the required dimensions within a certain tolerance.
- The embossed part is registered along with a coverplate; both are positioned in a hot press for a bonding cycle. The channels are now closed to form pipes through which the fluids can flow.
- The part is positioned and registered in the inspection stage, and inspected a second time.
- Functional testing is also possible, but it can only be conceived for a portion of the volume of achieved parts.

1.1.3 Tooling and equipment

To achieve the design shown in Figure 1.1 by the hot embossing process, two different tools have been used. The first one was conventionally micro machined from aluminum; the second one was hot-embossed from a silicon master made by DRIE to a bulk metallic glass (BMG). This latter method, developed at MIT by Hennan and Anand [7], has two main advantages: better accuracy of the shape reproduction and longer tool life. The tools and some SEM photos of features before embossing and after several hundred cycles are shown in Figure 2.

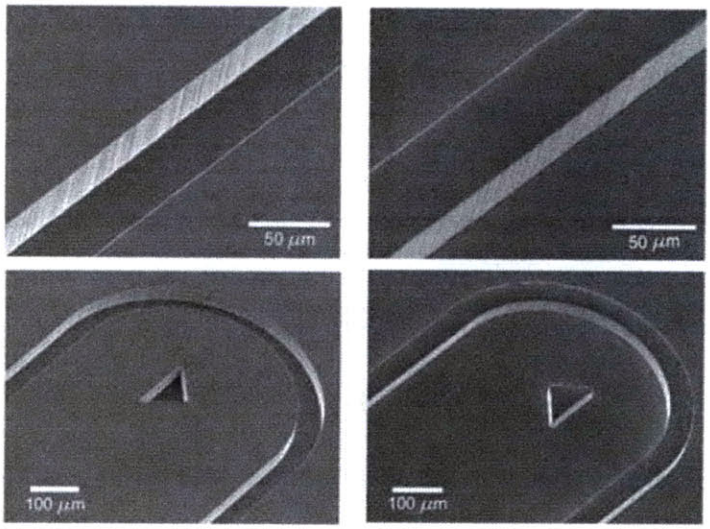

Figure 1.2: Channel and serpentine details
for a silicon master (Left) and Embossed BMG Tool (Right) showing
excellent reproduction fidelity (From [7]).

A low cost hot micro embossing machine has been developed with a 2 minute cycle time. Details can be found in [6]. Key features include a simple actuation system with limited travel, precise force control, rapid thermal cycling, and uniform heating. The platens are 25 mm x 75 mm in area, the size of a standard microscope slide. The entire stack assembly is shown in Figure 1.3 along with a photo of the overall equipment setup.

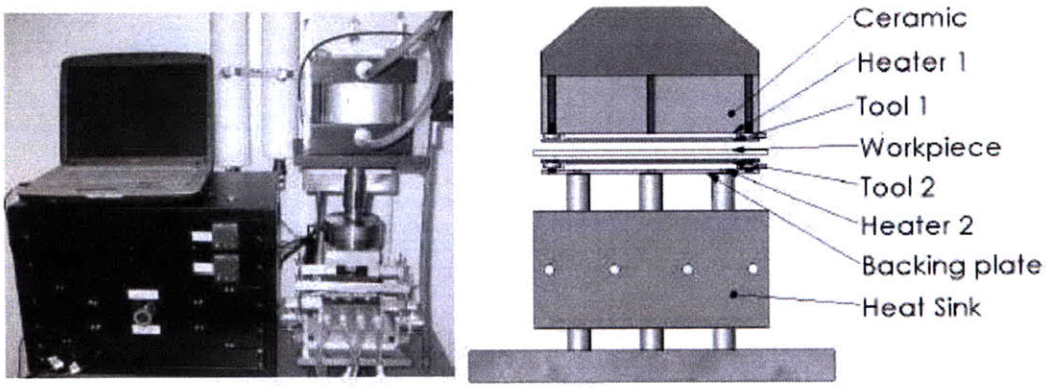

Figure 1.3: Rapid-cycle HME machine and the heater and forming stack.

To register the substrate in the hot embossing machine, a metallic carrier was originally used: the blank was inserted into this frame and then positioned in the work area by the interaction of magnetic pins on the machine with holes in the carrier (see Figure 1.4). This carrier was useful during the demolding at the end of the embossing cycle. Indeed, when the embossing tool decreases the pressure on the substrate, the latter tends to stay stuck to the mold. The carrier is held down to prevent the substrate pressed inside from following the upper platen. This solution had several disadvantages. First, the frame often doesn't carry the part before the embossing: it has to be large enough to encapsulate any blank, taking into account the tolerances of water jet machining for the frame and laser cutting for the blank. This means that the blank and the frame had to be assembled in the hot embossing machine. Secondly, the coupling of two pins into two round holes is either under constrained or over constrained, depending on the size of the holes: if the holes are large, the contact occurs on the cylindrical part of the pin and the coupling is under constrained; if the holes are small, the contact occurs on the hemispherical part of the pin and the coupling is over constrained. In any case, the positioning of the frame in the work area is not repeatable, and neither is the positioning of the blank in the frame due to the previous point. Finally, when the substrate is pressed into the carrier, it is difficult to remove it: a "disassembly" step is necessary, which has to be both strong and delicate to not damage the device.

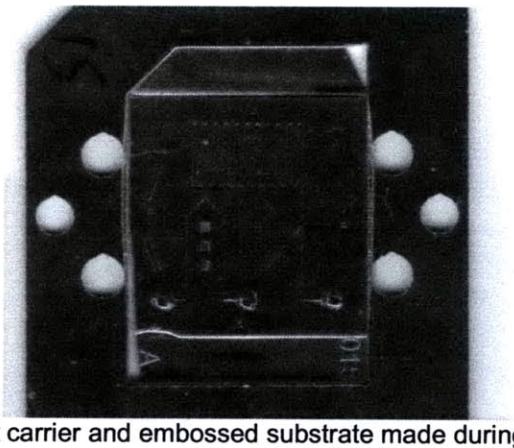

Figure 1.4: Part carrier and embossed substrate made during the µFAC project.

1.2 Objectives and structure of the thesis

1.2.1 Novelties of µFAC II

The goal of the *µFAC II* project is to design and operate a fully automated production cell including every processing step necessary to product a functional device.

The 3 most obvious stations are the hot embossing machine, the bonding machine and the inspection stage:

- The hot embossing machine is the same system than the one used for the *µFAC* project.
- The bonding machine is the station where the embossed substrate and the coverplate are assembled. The concept is similar to the embossing machine: with appropriate choices of temperature, pressure and holding time, a conventional hot press can achieve thermal bonding. This station hadn't been designed at the beginning of *µFAC II*.
- The inspection stage inspects the part at different times of the assembly, to detect any visual defects that would make the part unable to function: stereoscopy and motion-controlled super-resolution are used to create a 3D profile of the part (see [16]). A 3D

schematic of the inspection stage is shown in Figure 1.5. This concept is still in development.

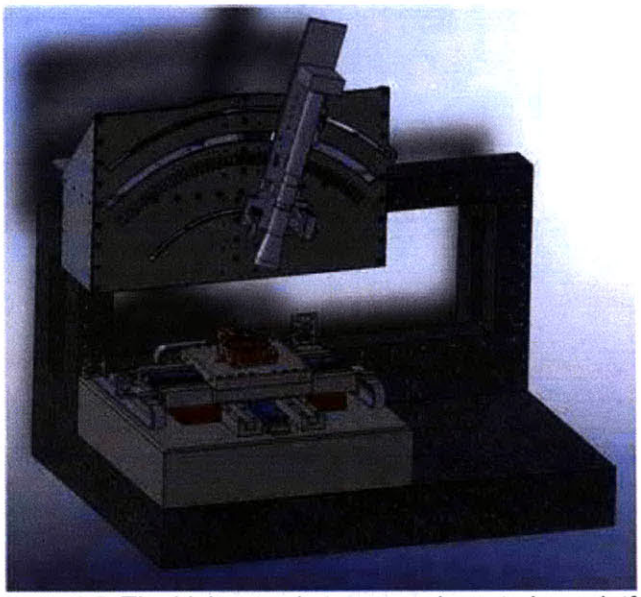

Figure 1.5: The high-speed stereoscopic metrology platform.

In addition to these stations, a part feeder has to be designed to store substrate blanks in a referenced location for delivery to the assembly: it can be considered the first station of the production cell.

A functional test setup will be integrated in the loop to operate on a small fraction of the production volume.

1.2.2 Objectives

The main objective of this thesis is to design and achieve a full automation of the μFAC cell. Several requirements are necessary to achieve this goal:

- Each station must be able to operate both independently and inside the production cell, depending on the situation: this means that the line must stay modular and adaptable to any possibility. The overall manipulation must be coordinated by a unique master controller that can delegate each task to the appropriate station when

the this station functions out of the line. As a result, two requirements appear. First, the master controller must be able to communicate with each station, but this communication should be made priority only when necessary. Second, the controller's overall material manipulation must be consistent and compatible with each station of the production cell, but must be replaceable by a manual handling of the parts.

- The production rate of the line has to be less than 5 minutes: it can be defined by the time between two insertions of blank material in the line, or the time between two exits of finished devices out of the line.
- Finally, and most importantly, the manipulation must be designed to enable the production of repeatable devices: the most critical parameter for that purpose is the positioning of the part into the different stations. To get an idea of the magnitude of acceptable uncertainty, remember that the width of a channel is 40 microns: the error in position must be a fraction of this distance. This objective strongly depends on the fixturing strategy: actually, finding an alternative to the original metallic part carrier described in section 1.1.3 was one of the first motivations of this thesis.

We will first examine different scenarios of large-scale manipulation: the macro scale manipulation in the production cell is presented in Chapter 2. Consistency and modularity are considered. After that, the small-scale manipulation will be thoroughly studied for repeatability and adaptability purposes in Chapter 3. In these two first chapters, design ideas and realized solutions will be explained. Then in Chapter 4, an analysis of the manipulation strategy is presented. The next chapter explains the challenge of the part feeder and the solution found to answer this issue. Chapter 6 shows how the communication in the production cell has been implemented and will characterize the efficiency of the factory. Finally, Chapter 7 is a close study of the flow of material in the production cell and an optimization of the production rate.

Chapter 2.

Large-scale positioning

2.1 Concept of positioning

As described in [17], there are three ways to organize an assembly system. In a synchronous system, the products are simultaneously indexed to individual machines that operate at a fixed frequency. Alternatively, the length of a task depends on the machine in non-synchronous systems: buffers are used to fill the time gap and decouple two machines. Finally, in continuous systems the product is no longer discretized.

A continuous model does not fit our devices. A synchronized system would waste precious time, since the length of the cycle time varies largely between the hot embossing machine and the inspection stage. The machines used in the production cell and the product fit an asynchronous model. We will discuss in Chapter 7 the use of buffers, and only consider the choice of manipulation in this section.

The manipulation and positioning consists of picking up a part from a machine upon process completion (when the part is ready for manipulation) and placing it with good repeatability in the next station, for each pair of adjacent stations. We want to maximize system throughput, so we would like this manipulation to occur as soon as possible after the part becomes ready for manipulation. However, since the system is asynchronous, it is possible that the processes at two different stations finish and are ready for unloading at the same time: for example, if the hot embossing and the bonding are completed at the same time. The geometries of the working areas of the stations differ from one other and have small clearances: for example, the opening between the jaws of the bonding machine has a height of 3/8" while the demolding fingers in the

hot-embossing machine (between which the 34 mm-long part has to be inserted) are only 38 mm apart.

These considerations have led us to consider different options of manipulation, each having advantages and disadvantages.

2.1.1 Multiple independent manipulators

The first option consists of making each manipulation independent from the others. It could be achieved with multiple manipulators, each one being dedicated to a pair of process stages. It would be adapted to the travel between these two adjacent workstations, and it would need a reduced workspace to reach only those stations. Its task would be simple and repetitive, independent from the other manipulators and allowing two different manipulations to happen at the same time.

However, this option also has the disadvantage of multiplicity: from a global point of view, every feature would be multiplied. Economically, the cost would be multiplied. The footprints of each manipulator, though they are small, would be added, creating an obstruction of the global workspace. Even from a designer viewpoint, each one of the three or four manipulators would have to adapt to two machines, in contrast to one manipulator adapted to three machines: thus, even if each manipulation would be simpler, the simplification might not be large enough to justify three designs instead of only one.

2.1.2 Unique manipulator

The second option consists of one manipulator sitting in the center of the production cell and transferring the parts from one machine to another. The manipulator needs to interact with each of the different geometries of the work areas and to reach all of them. The investment in time and money, instead of being divided among several manipulators, would be entirely devoted to one: thus it can be expected that its features will be consequently enhanced.

We considered two different types of robot commonly used in the industry, categorized by their number of axes of motion.

- 6-axis robot: articulated arm:

Figure 2.1 a is a model of a robot 6 axes: the first axis A1 is the prime mover, it rotates the whole body of the robot; the second and third axis extend the arm; the sixth axis rotates the end-effector; the fourth and fifth axes allow the arm to pickup a part that is not necessary parallel to the floor and to flip it, which means that all type of motion is possible.

- 4-axis robot: SCARA:

A SCARA robot is shown in Figure 2.1.b. SCARA stands for **S**elective **C**ompliant **A**ssembly **R**obot **A**rm. Three of its axes of motion are rotational, one is vertical. The 3 rotational axes can be described as the shoulder, the elbow and the wrist of the arm: they only allow a horizontal motion, which is thus fully decoupled from the vertical motion. SCARA are fast and typically compact.

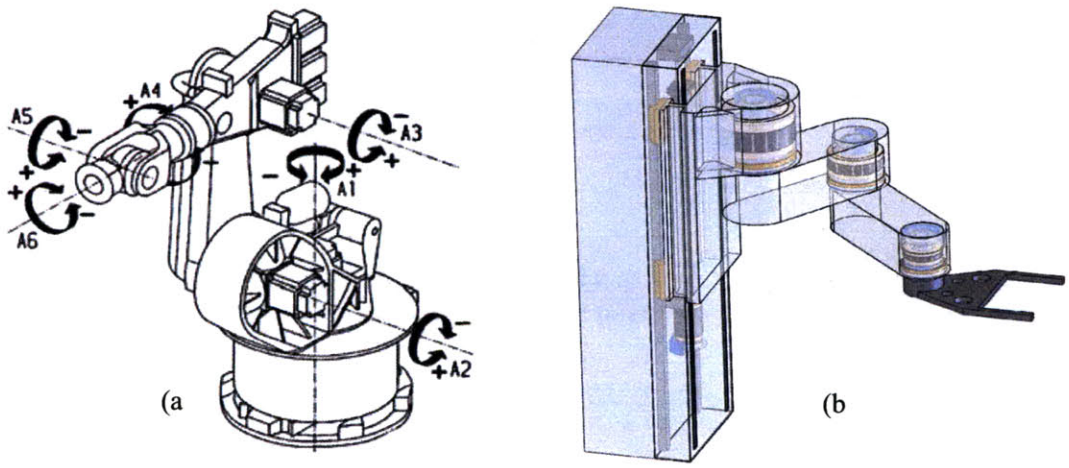

Figure 2.1: Models of 6-axis robot (a) and the SCARA robot (b)

Since all the work areas of the stations are horizontal and don't require the part to be flipped or tilted, 6 axes of motion are not necessary. Moreover, it is known that the repeatability in position decreases when the point of interest moves away from the center of the workspace of the

robot (see section 2.2). This is to say that we want the areas of manipulation to be as close as possible to the robot. We select a SCARA manipulator because of this last parameter.

2.2 Layout of the factory

To select a SCARA manipulator that best matches the requirements of the production cell, it is necessary to know how the machines are arranged in the cell. Of course, the arrangement will be chosen so that each work area is reachable and gets the best possible repeatability.

Since a SCARA robot has been chosen, the coordinates X and Y of the position of the end-effector in the horizontal plane are:

$$\begin{pmatrix} X \\ Y \end{pmatrix} = \begin{pmatrix} l1\cos(q1) + l2\cos(q1+q2) \\ l1\sin(q1) + l2\sin(q1+q2) \end{pmatrix} \quad (1)$$

where l_1 and l_2 are the length of the arms and the q_1 and q_2 are the rotation at the joints. q_1=0 when the first arm is aligned with the x-axis. q_2=0 when the second arm is aligned with the first arm.

Then, assuming that each joint has a error in rotation of dq_i, where i=1,2, it's easy to see that the resulting error in end effector position is

$$\begin{pmatrix} dX \\ dY \end{pmatrix} = \begin{pmatrix} -l1\sin(q1) - l2\sin(q1+q2) & -l2\sin(q1+q2) \\ l1\cos(q1) + l2\cos(q1+q2) & l2\cos(q1+q2) \end{pmatrix} \begin{pmatrix} dq1 \\ dq2 \end{pmatrix} \quad (2)$$

That is to say

$$\begin{pmatrix} dX \\ dY \end{pmatrix} = J \begin{pmatrix} dq1 \\ dq2 \end{pmatrix} \quad (3)$$

where J is the Jacobian of the motion.

Since J strongly depends on the desired position of the end-effector by $q_1$and q_2, the accuracy of the robot can be computed in its entire workspace.

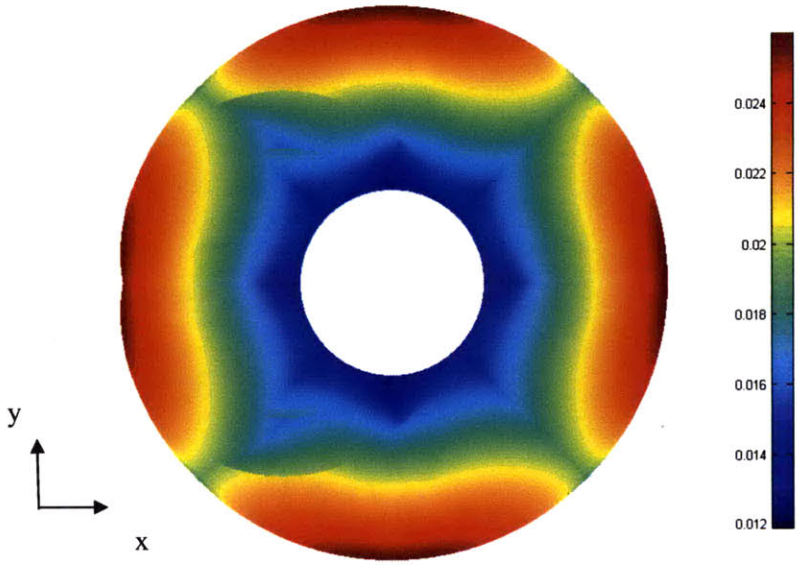

Figure 2.2: Expected error in position of the endpoint (mm)
for an angular precision of 1.7x10-3 deg for each joint, in the workspace of the robot SCARA.

In Figure 2.2, one shows the maximum possible error in position for each point in the workspace of the SCARA robot. For each position, there are several solutions for ($\mathbf{q}_1$, $\mathbf{q}_2$): the error shown in Figure 2.2 is the maximum of these possible errors:

Error(X,Y)=max(Error($\mathbf{q}_1$, $\mathbf{q}_2$)) for any ($\mathbf{q}_1$, $\mathbf{q}_2$) who satisfies the equation 1.

The biggest error is in red and at the periphery inside of the disk; the smallest error, in blue, mostly stands in the ring the closest to the center, but is also on the first and second bisector of the x-y axis.

We can roughly check that the computation seems reasonable by a consideration of the norms:

$$error\ in\ position \leq \sqrt{2}\ (error\ in\ rotation)$$

$$\|J\|^2 = l_1^2 + 2l_2^2 + 2l_1 l_2 \cos(q_2) \leq l_1^2 + 2l_2^2 + 2l_1 l_2 \qquad (4)$$

Notice that the disk isn't complete on the left most region of the workspace. Since the joints don't have a range of ±180°, some points can not be reached. For the same reason, the inner disk where the robot stands is larger: its radius is

$$\sqrt{l_1^2 + l_2^2 + 2l_1 l_2 \cos(q_{2max})}$$

instead of $\| l_1+l_2 \|$.

2.3 Safety

An industrial robot is a powerful instrument: it is strong and fast and can be lethal to anyone getting in its way. That's why appropriate safety measures are necessary to make sure that nobody can enter the workspace of the arm when it is moving.

Two barriers can be considered: physical or virtual. A physical barrier would prevent anybody from entering the workspace: it could be a high fence or a rope pulled all the way around the dangerous area. A virtual safety barrier is an invisible system that shuts the robot off whenever somebody enters the workspace: the basic principle is to detect the presence of a person in the area. This can either be done by securing a perimeter or the whole area: the industrial solutions go from a safety light curtain to a safety mat. Physical and virtual barrier safeties can be combined: for example, a solution often used in the industry consists of a high fence with a door whose lock is connected to the controller of the robot. If the door is open, the robot is disabled. For any of these solutions, an emergency button or a "dead man's switch" has to be added: for the first one, the system is shutdown when the operator presses the button, for the second it is shutdown when the switch is released.

2.4 Application of the concepts

2.4.1 Robot

As is stated in 2.1.2, we chose to use a SCARA robot. Its arm length had to be chosen using the analysis of the SCARA position repeatability. For a given arm length, the machines, whose dimensions are known, have to be arranged to minimize the overall error of position. The chosen arm length is the smallest that can match both arrangement and minimal error in position requirements. The layout of the production cell is shown in Figure 2.3 and described in 2.4.3.

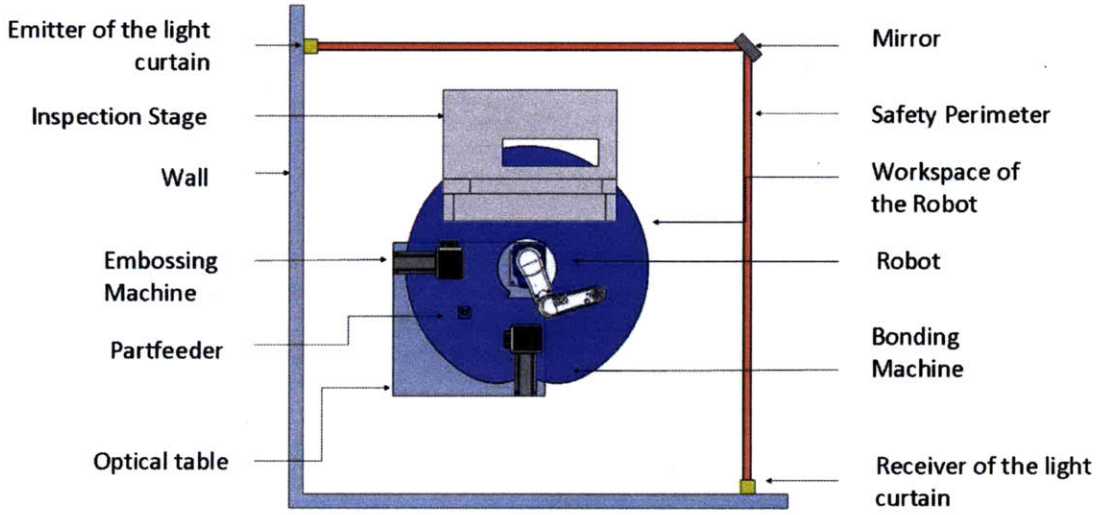

Figure 2.3: Layout of the production cell

The SCARA that we chose is an Epson G10-85, along with the Epson RC180 controller. Their complete specifications can be found in [18] and [19] and are summarized in Table 1 and Table 2. A picture of the manipulator is shown in Figure 2.4.

Arm length (mm)	J1	450
	J2	400
Payload (kg)	Max/rated	10/5
Repeatability	J1+J2	±0.025mm
	J3	±0.010mm
	J4	±0.005deg
Cycle time w/2kg (sec)		0.369
Max Operating Speed	J1+J2	11000 mm/sec
	J3	2350 mm/sec
	J4	2400 deg/sec
User Lines		Electric (24 lines), Air (4 lines)

Table 1: Summary of the specifications of the G10-85 Epson

Joint Control	Up to 6 joints simultaneous control
Motion Type	Continuous Path, Point to Point
Speed/Acceleration/Deceleration	Fully programmable
Teaching Method	Remote, Direct, Manuel Data Input
Digital I/O	16 Inputs/8 Outputs (optically isolated)
Communication Interfaces	Ethernet, USB

Programming Language	SPEL+ Lite (functions, parameter passing, variable types, error handling…)
PLC connection	Easy to use controller as PLC slave through DeviceNet, Profibus, EtherNet/IP or remote I/O Connection

Table 2: Summary of the specifications of the RC180 Controller

Figure 2.4: Epson SCARA G10-85

2.4.2 Safety

Due to space constraints, a physical fence is not the best or even cheapest solution. We chose a light curtain to secure two edges of a virtual square around the workspace of the robot. The perimeter is then completed by the walls of the room, as shown in Figure 2.3.

We chose the SF4B-H36 model along with the SF-C13 safety relay from Sunx. Table 3 summarizes their specifications. The light curtain, the safety relay and the emergency stop function of the controller were wired accordingly to the wiring diagram shown in Figure 2.5.

SF4B-H36		SF-C13	
Number of beam channel	36	Supply voltage	24V DC
Sensing range	0.3 to 9 m	Current consumption	100 mA or less
Beam pitch	20 mm	Pick-up delay	Auto reset: max 80 ms Manuel reset: max 90 ms
Protective height	710 mm	Response time	10 ms
Current consumption	Emitter: 80 mA or less Receiver: 115 mA or less		
Min. sensing object	Opaque object of 25 mm diam		
Effective aperture angle	±2.5 deg		
Supply voltage	24V DC		
Response time	ON to OFF: max 14 ms OFF to ON: max 90 ms		

Table 3: Specifications of the SF4B-H36 light curtain and the SF-C13 safety relay

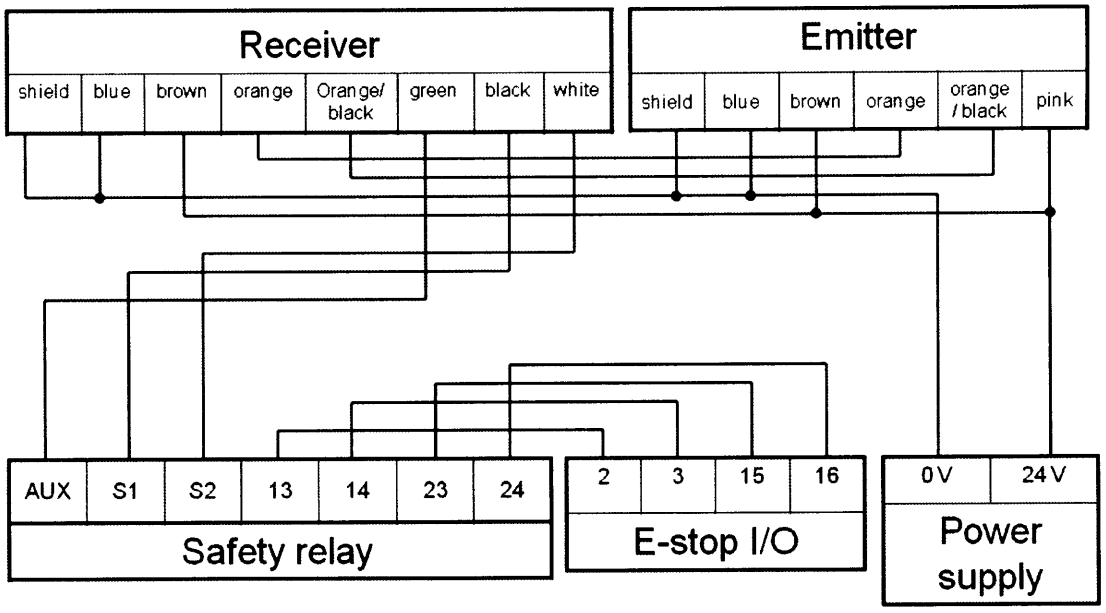

Figure 2.5: Wiring diagram of the light curtain and safety relay to the controller

2.4.3 Layout of the factory

The resulting layout of the factory is shown in Figure 2.3.

The hot embossing machine, the bonding machine and the robot are mounted on an optical table. This latter provides a precise metric grid of holes with 25 mm spacing. We built the legs of the table from aluminum extrusions, to provide a structure that prevents the table from shaking while the robot is moving. Also notice a part feeder, the first station of the production cell. Its design and the analysis of its efficiency will be discussed in Chapter 5.

2.5 Summary of the large-scale manipulation

Decision	Selected solution
Scenario of manipulation	Unique manipulator (2.1)
Type of manipulator	SCARA 4 axis 850 mm arm length (2.2 and 2.4.1)
Safety principle	Virtual barrier (2.3)
Virtual barrier	Light curtain (2.4.2)

Table 4: Summary of the selected solutions for the large-scale manipulation

Chapter 3.

Small-scale positioning

3.1 Manipulation strategy

The specifications of the manipulator are fixed. Next, the manipulation strategy must be designed, taking into account the characteristics of the component. Our part is made of plastic; its overall shape is deformable and relatively flat; it is small, light and fragile. The manipulation consists of two seemingly different concepts that actually strongly depend on each other to allow consistent and repeatable manipulation. The first one, which can be called the handling principle, answers this question: what force or strategy should be chosen to handle the part from one point to another? The second one is the fixturing principle: how will the part interact with the stations? Thus, we want to choose the handling and the fixturing principles to be compatible with each other and with each step of the assembly process.

3.1.1 Handling Principles

A good review of the handling principles that can be used for parts of this size range is presented in [20]. Electric and magnetic attractions won't work for the PMMA part by itself, but could be used if a metallic part were added in the fixture of the part and the coverplate. A vacuum tool or a gripper would work in any case. [21] compares both solutions in the case of microassembly, whose repeatability requirements are similar to ours. A gripper is a well known solution, widely used in the industry. It can be purchased off the shelf and requires a force or a displacement control. On the other hand, a suction tool only works with flat or deformable parts, but is cheap and works well with fragile parts. To read more about the range of applications using a suction handling principle, see [22]: for example, the suction principle fits very well in

the fruit or the textile industry, as well as the Printed Circuit Board Assembly. It also has the advantage of decoupling the vertical motion and the horizontal motion, which is consistent with the selected large-scale manipulation strategy.

3.1.2 Fixturing Principles

It is necessary to decide how the part interacts with the stations; this is to say how it will be held during the steps and how it will be aligned with the tools. First we have to better understand what happens to the part during the processing steps.

During the hot embossing step, the PMMA blank is heated and squashed, and some melted material will tend to flow in a non-repeatable way. It is important to notice that if the embossing tool is smaller than the blank, the embossed area will be thinner than the rest of the part; if on contrary the embossing tool is larger than the blank, the finished part will have a homogeneous thickness, smaller than the original thickness of the blank. But although the homogenous thickness is desirable, having a tool larger than the blank creates difficulties during the demolding step. Based on the design of the fluid mixer, the holes need to be connected to the channels to allow the fluids to flow. The diameter of the laser cut holes (1.5 mm) is much larger than the width of the channels (50 μm) so that the alignment of the holes with the embossing tool doesn't have to be very accurate.

Then, during the bonding step, a PMMA coverplate is pressed against the embossed surface of the substrate. Since the coverplate is blank, its only real requirement is to cover uniformly the whole embossed area, but for more complicated products, we would have to precisely align the patterns of the coverplate and the embossed part.

Also notice that if a non-deformable frame is selected, it has to effectively carry any blank from the beginning to the end of the assembly, and an assembly step should also be added to fit the blank inside the frame. The clearance of the rectangular hole in the frame has to be large enough to fit any blank and tight enough to carry the part from the edges (the bottom side of the blank should be free to be heated during the embossing step). The only possible way to

overcome all these constraints is to design the dimension of the clearance hole to be the same as the blank's dimensions, and to force the blank to fit into it by pushing it vertically.

Thus, several strategies seem to be possible, depending on what we decide to be the reference of alignment. If we decide to enclose the part in a non deformable frame, the edge of this frame will become the reference. If on contrary we decide to not use any frame, the reference will have to be a feature on the part itself: we could either add a manufacturing step to include this feature or use one of the existing steps. The easiest solution is to create this feature during the embossing step, either on the edge or on the surface.

3.1.3 Decision tree and resulting manipulation strategy

To help to choose the most satisfying combination of handling and fixturing strategies, we draw a decision tree (Figure 3.1). Each branch represents a decision and each leaf is the consequence of a decision.

From this decision tree we conclude that the best choice is to combine a suction tool and a reference on the edge of the part, created by a corner during the embossing step. No frame will be used. To align this reference on the part to the other stations, the kinematic coupling theory (see [23]) states that only three points are necessary. Thus we will add three pins or balls to the workspace of any station down the line. Every corner should be created with the same repeatability as the embossed features by the embossing machine: then, if we can align the part corner to the pins with a better repeatability, the embossed features will be positioned in the stations with the same repeatability as for the embossing.

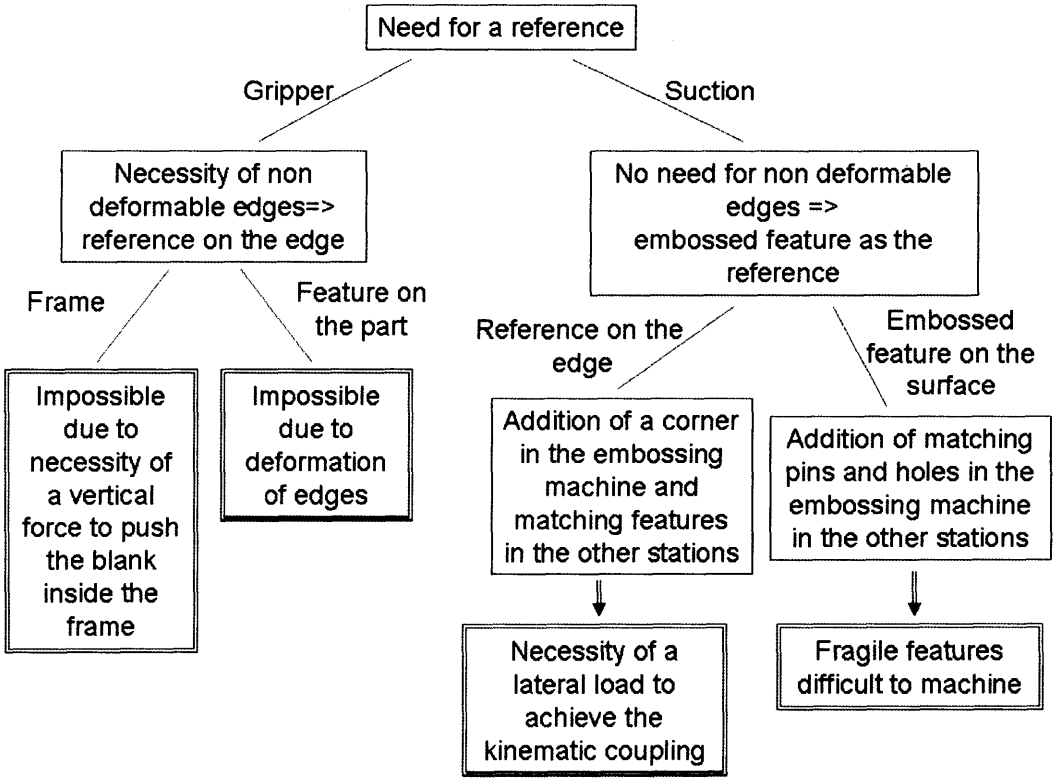

Figure 3.1: Decision tree for the combination of fixturing and handling strategies

The only resulting requirement of this decision is to produce a lateral load to push the part against the pins. Since the position of the part before being pushed is not known with certainty, a constant displacement of the arm (open loop) is *a priori* not possible to produce this lateral force: if the displacement were too large, it would destroy the part or the pins; if the displacement were too small, the contact might not be reached. A new function of the end effector is thus necessary. We could use sensors to control the horizontal force in a closed loop: the complexity of it could certainly be achieved, but easier alternatives should be considered. For example, we could use compliant components to "absorb" the uncertainty of position of the part; even if it is pushed further than necessary, the compliant component will be deformed before the part, thus producing a roughly constant load in a certain range of displacement. Compliance has been widely used in robotic applications, as described in [24].

The final manipulation strategy is summarized in Figure 3.2.

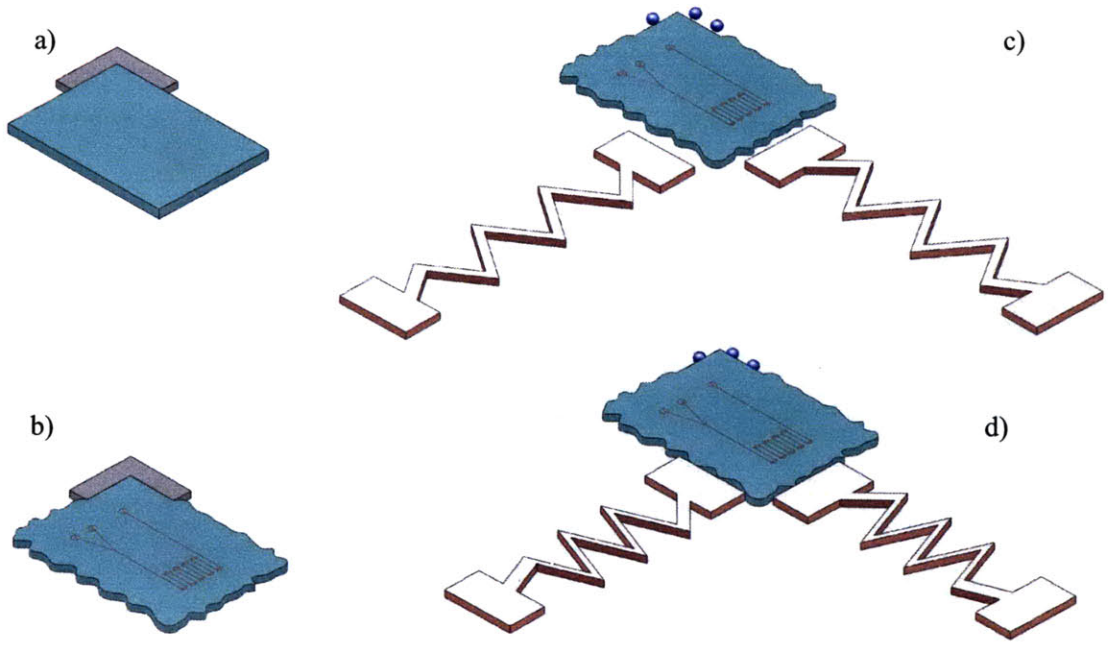

Figure 3.2: Schematic summary of the manipulation strategy
a) before embossing - b) after embossing- c) placed on another station- d) pushed against the pins

The part is first placed in the hot embossing machine against the corner (Figure 3.2 a), then the features are embossed on the part while a clear edge is created (Figure 3.2 b). The rest of the edges are deformed. The embossed part is then picked from the hot embossing machine using the suction tool of the end effector (not shown in the figure) and placed on the next station close to the pins but not yet in contact (Figure 3.2 c). The compliant component of the end effector, shown in schematic form as a spring, is idle and not deformed. The end effector itself, to which the compliant spring is attached, is not shown on the figure for clarity purposes. Finally the part is pushed against the pins: the compliant component is compressed and a constant load is applied on the part (Figure 3.2 d).

Notice that, as another consequence of this decision, the original μFAC mechanism used to hold the part carrier and the substrate down during demolding can no longer be used, since the

part carrier is no longer present in the fixturing strategy. To respond to this issue, a new solution has been designed for the hot embossing machine (see Figure 3.3): two demolding fingers will prevent the embossed substrate from following the mold on the upper platen when the latter releases the pressure and comes up. As a result, the blank has to be inserted below these fingers and pushed against the corner before the embossing, and the embossed substrate has to be slid out of the work area after the embossing. This makes the manipulation a little more complicated but assures the consistency of the overall strategy.

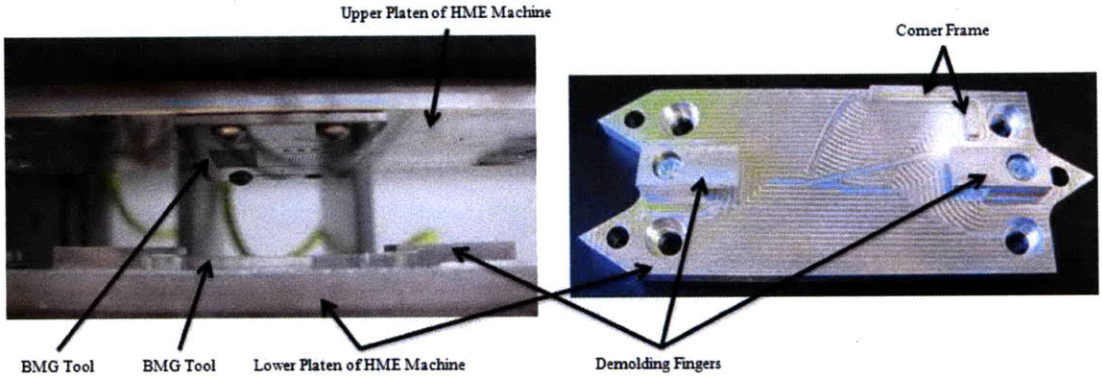

Figure 3.3: The tooling side of the HME machine showing the BMG tool, the corner frame and the demolding fingers.

3.2 Design of the end effector

3.2.1 Vacuum circuit

To get a proper suction tool, a few requirements are necessary:

- We need a vacuum circuit operable by the controller; this is to say that the suction cup or vacuum chuck has to be actuated by a vacuum that can be turned on and off as an output of the robot. This is typically done with a solenoid valve which is actuated by a power supply.
- The vacuum level has to be regulated: too much vacuum could damage the features on the part, but the part won't be lifted if the vacuum level is too small.
- The air circuit has to be filtered to protect the part from contamination.

- We want to know if the part has actually been picked up or not. A vacuum switch can be set to feed back a digital signal to the controller: 0 if the vacuum is below a chosen level (in absolute values), 1 if it is above.
- The tubing and equipment needs to have a minimal footprint. The use of the robot's air lines thus seems reasonable.

A schematic figure of the vacuum circuit including the part numbers of its components (from Tuthill and SMC) can be found in Figure 3.4.

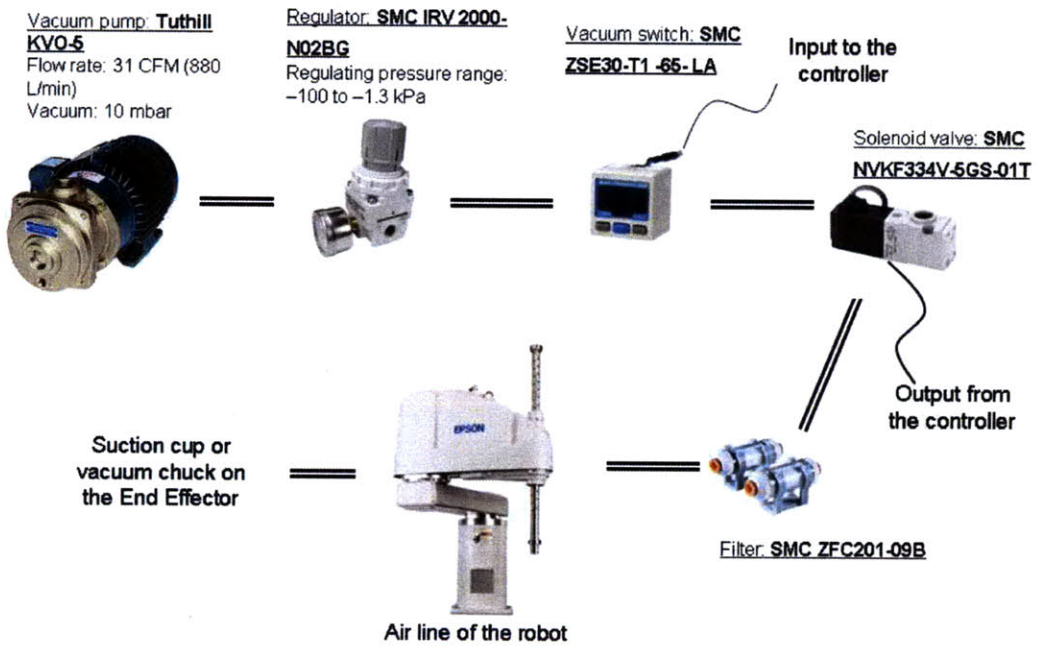

Figure 3.4: Schematic vacuum circuit

3.2.2 *End effector*

As stated earlier, the end effector has to carry out two functions: the pick and place and the alignment. The pick and place function is provided by the suction tool while the alignment is accomplished by the compliant component. They are ideally orthogonal to each other since the suction should only imply a vertical motion as opposed to the horizontal alignment occurring on a surface. This statement will be tested in the section 4.2.

Two versions of the suction tool have been designed: their height is strictly constrained by the spacing between the jaws of the machines. Indeed, the pneumatic cylinder providing the pressure necessary in the embossing and bonding processes has only a limited travel range. Since the end effector has to be inserted between the maximally opened jaws between which the part is placed, heated and pressed, its height strongly depends on the travel range of these cylinders.

3.2.2.1 Suction pad end effector

The first end effector was designed before the bonding machine was completed. The maximum opening of the bonding machine was unknown and assumed to be the same as the hot embossing machine: about 5 cm. A tiny off the shelf suction pad was selected as the suction tool.

The end effector is attached to the quill of the robot, a 25 mm diameter cylinder. This cylinder is inserted into a matching hole drilled in the end effector; both are then fixed by side screws.

The suction pad design is simple and doesn't include the alignment function. It is shown in Figure 3.5. It is only comprised of a suction pad (SMC ZPY08US-N6-B5) and a contact switch, whose function and characteristics are discussed in section 3.3.1.

The minimum diameter of the suction pad has been found using the well-known formula [26]:

$$D = 11.2 \cdot \sqrt{\frac{m \cdot s}{P_u \cdot c}} \qquad 5$$

Where

- D is the diameter in mm,
- m is the mass of the object to lift in kg: 0.1
- s is the safety coefficient (at least 2),
- Pu is the available vacuum pressure in bar : 0.8
- and c is the number of cups:1.

The minimum diameter is calculated to be 5.6 mm. Thus a diameter of 8 mm should provide a good safety margin. The height of the suction pad is 44 mm: it would fit between the jaws of the hot embossing machine.

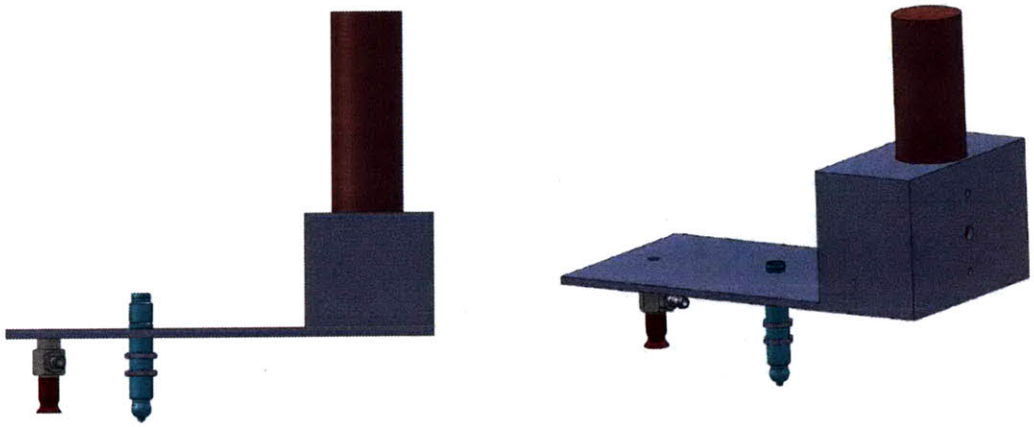

Figure 3.5: 3D representation of the suction pad end effector

3.2.2.2 *Vacuum chuck end effector*

It appeared later that the spacing between the jaws on the bonding machine was actually only 1.6 cm, as opposed to the original 5 cm that the end effector was designed for. To solve this problem, a custom vacuum chuck was designed and machined to be the new end effector.

Several constraints have to be taken into account in this new design:

- As stated earlier, the end of the vacuum chuck has to fit into an opening of 1.6 cm.
- There should be enough space between the end effector and the jaws to allow a vertical pick and place, as well as a horizontal alignment of the part.
- The horizontal and vertical movements corresponding to alignment and pick and place should be decoupled: the component of the end effector dedicated to one function should not touch the part while the other is working.
- The air line coming from the robot, which is used to create the vacuum, has a 6 mm diameter.
- The surface area of the holes through which the vacuum is in contact with the part has to be big enough to lift the part (see Equation 5).
- There must be compliance in the vacuum chuck surface in order to pick both flat and warped parts.

To satisfy these requirements, the end effector shown in Figure 3.6, Figure 3.7 and Figure 3.8 was designed.

A manifold makes the connection between the air line and the vacuum chuck itself: its role is to split the 6 mm diameter hole into several smaller channels precisely machined into a long, thin aluminum plate (the vacuum chuck). The connection between this component and the plate is sealed to avoid any air leaks. Several holes arranged in a diamond pattern are drilled into the plate orthogonally to the channels: they form the vacuum chuck. A thin layer of foam is added on top of that pattern to allow a slight vertical compliance.

The compliant fingers are made of closed-cell foam covered by a Teflon anti-friction tape. This combination of very soft and compliant materials provides quick recovery as well as a

minimum friction between the end effector and the PMMA part. Their shape has been designed to enable them to touch the part on specific locations, which gives a better sense of the interaction occurring.

The vacuum chuck is far enough from the fingers to make sure that the fingers won't touch the part when it's picked up. The fingers are slightly thicker than the chuck: when they align the part, the end effector is placed higher than when it is picking the part, and the chuck doesn't touch it.

The vacuum chuck is attached to the robot in the same manner as the suction pad.

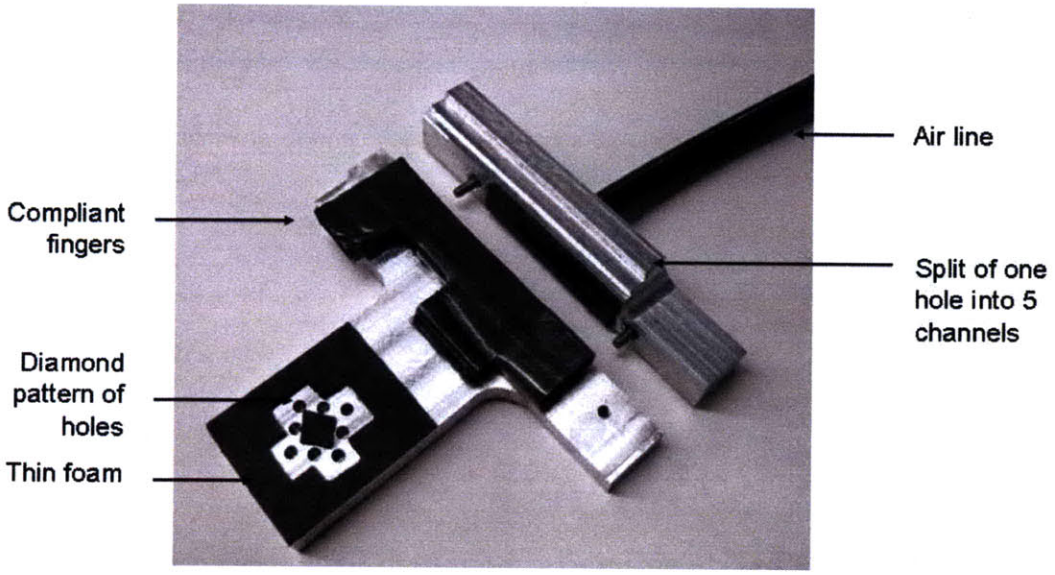

Figure 3.6: Exploded view of the vacuum chuck design.

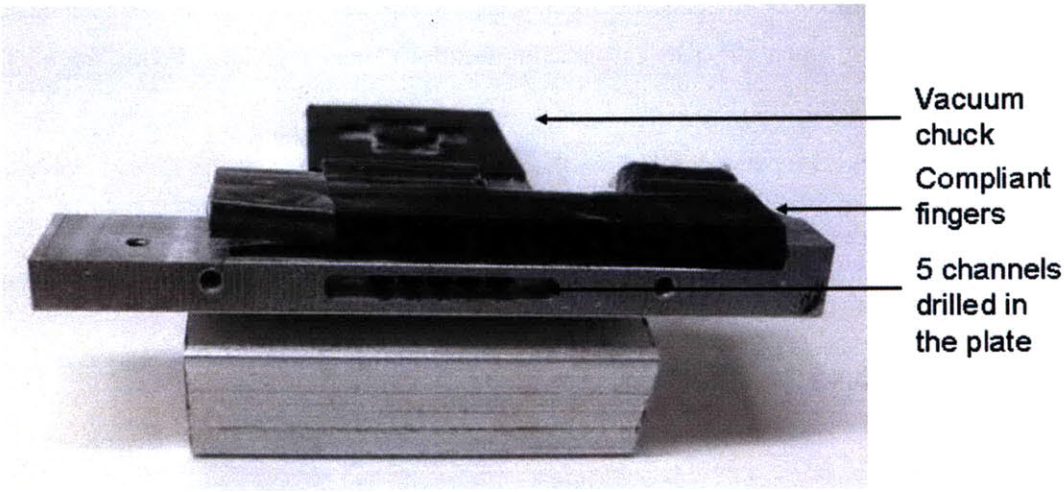

Figure 3.7: View of the vacuum chuck showing the channels precisely machined in the surface of a plate.

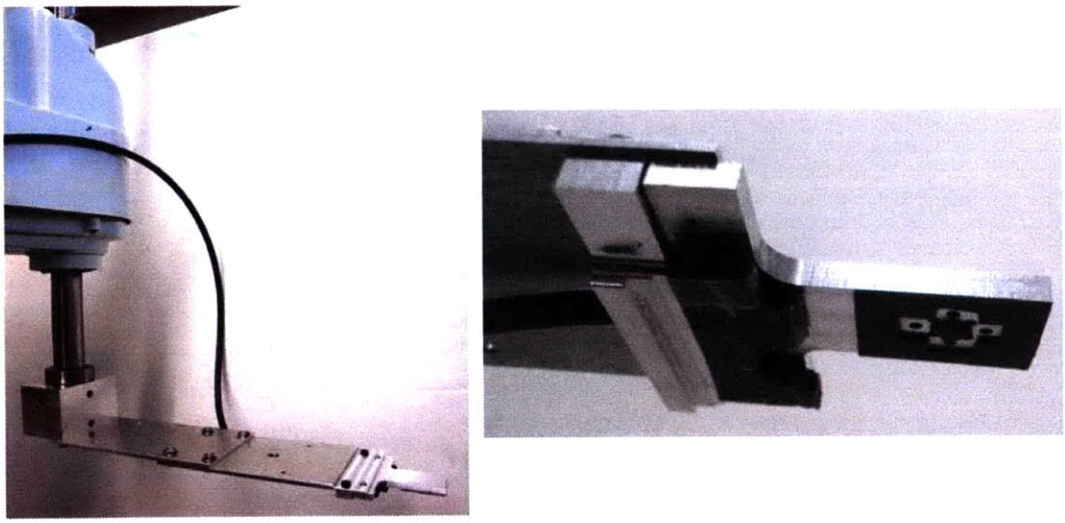

Figure 3.8: Global view and detail of the vacuum chuck end effector

3.3 Control of the manipulation

3.3.1 Sensors

To improve the repeatability of the manipulation, two sensors are used.

The first one has already been described in 3.2.1: it is a vacuum switch. This sensor has 0.2% repeatability and sends a digital signal indicating if the vacuum level goes above a certain value, this is to say if the part has been picked up. It is particularly useful in the event of an error: for example if there is no part in a station, if it is stuck or if it is not at the expected position. Checking for the part in these cases will prevent any further manipulation that could possibly damage the equipment.

The second sensor is the contact switch mentioned in 3.2.2.1. This sensor helps during the pick and place process to reduce the vertical uncertainty. It sends a digital signal indicating when the tip of the precision switch is in contact with something. The selected product is made by Baumer Electrics (MY-COM M75P/S35L): it has 1 μm accuracy, with an activating load of 75 cN. It is shown in Figure 3.9. We attach it to the end effector in a vertical position. At the last step of the picking or placing process, the arm has a slow vertical motion; we program it to go down to a point lower than required, but to stop when the contact is made, which is set to occur before this low point is reached. With this strategy, the vertical repeatability of the arm is improved from 10 μms to 1 μm.

Figure 3.9: Precision contact switch

3.3.2 *Torque monitoring*

Again, the robot is really powerful and could damage the machines in the event of incorrect manipulation. It is important that whenever the arm reaches an obstacle in its trajectory it stops and does not try pushing through the obstacle, especially when it is in the confined and restricted area of the workspace of the machines. In order to protect the equipment, another control is necessary, which will use the manipulator's existing sensors. Unfortunately they don't provide information such as force or torque, but rather current or voltage. It is thus required to calibrate these values in order to know the value corresponding to the maximum torque that should be applied when the end effector is in a critical area. This value should be superior to any torque value applied during a normal operation, but inferior to the values of torques when the end effector reaches an obstacle. It implies that the joints have to operate with a small acceleration, thus a small speed, which makes the manipulation slower. Once the maximum torque value is defined, the torque monitoring can be conducted. By a simple command of the controller language, we constantly have access to the torque applied to each joint; when this torque (or rather the coded value of this torque) goes above the defined value, any operation of the robot stops.

3.4 Summary of the small-scale manipulation

Decision to make	Selected solution
Handling strategy	Suction (3.1.1 and 3.2.1)
Fixturing strategy	Kinematic coupling of an embossed corner and a set of three pins (3.1.2 and 3.2.2)
Suction tool	Suction pad and vacuum chuck (3.2.1 and 3.2.2)
Alignment tool	Compliant fingers (3.2.2.2)
Control of the positioning	Vacuum switch and precision contact switch (3.3.1)
Control of the force	Torque monitoring (3.3.2)

Table 5: Summary of the solutions selected for the small-scale manipulation

Chapter 4.

Analysis of the self-alignment strategy

Once the end effector and the vacuum circuit are designed and ready to operate, it is possible to test the repeatability of the selected manipulation strategy. First, the repeatability of the suction function without any manipulation from the robot, and then each step of the alignment strategy, from the easiest to the closest to a real situation of manipulation are analyzed.

4.1 Measurement platform

To analyze the repeatability of any manipulation, a precise knowledge of the part's position is necessary. The absolute position doesn't need to be known to test repeatability, (as opposed to test accuracy), but the relative position in a certain referential is important. The uncertainty related to the measurement of this position must be negligible or at least less than the error in position repeatability in order for us to be able to analyze the repeatability.

A measurement platform has been designed (Figure 4.1). The concept is simple: a square of transparent material is held by four rods screwed onto the optical breadboard. We carefully adjust the height of each rod (which is made possible by the adjustable attachment of the platform to the rods) to get a horizontal surface. The part will be picked and placed on this surface. A camera stands below the platform and takes images of the part through the transparent surface. The chosen camera is the handheld microscope DinoLite AM413T. The magnification can go continuously from 10x to 200x. Its resolution is 1280 by 1024. It is directly plugged to a computer by a USB port. With the maximum magnification, it is not possible to see the entire part: the field of view has only a dimension of a couple of mm^2. The camera will take images of a detail inscribed on the part: a cross has been drawn with a needle on a blue layer of varnish

deposited on the surface to get a better contrast. A picture of the measurement platform is shown in Figure 4.1and an example of images of the cross taken by the camera is in Figure 4.2.

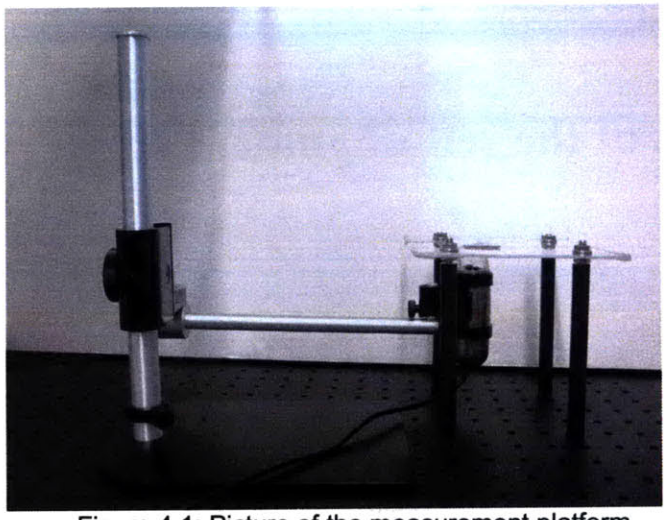

Figure 4.1: Picture of the measurement platform

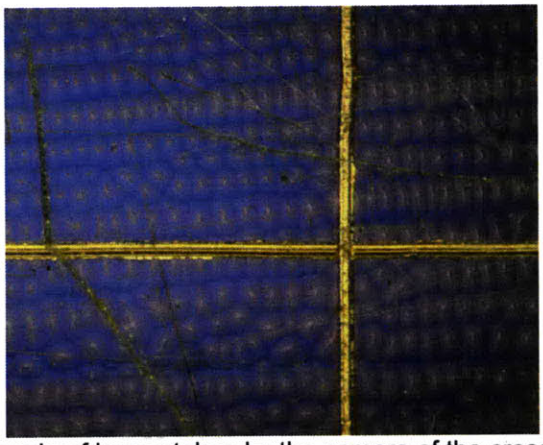

Figure 4.2: Example of image taken by the camera of the cross detail through the measurement platform

Since neither the camera nor the platform move, knowing with accuracy how the cross moves inside the images would provide enough information to deduce the repeatability of the manipulation. To detect the position of the cross, an algorithm based on image processing has been developed. The principle and details of this algorithm are provided in the Appendix, as well

as the analysis of its efficiency. It resulted that its sensitivity in position is better than the size of a pixel: for a focused image at maximum magnification, it is about 1.75 microns. The angular resolution has been determined to be less than 0.02 deg.

4.2 Pick-and-place with the suction pad

4.2.1 Experimental procedure

The goal of this experiment is to determine the repeatability of the pick and place process by itself and to prove that the uncertainty in position of the suction tool can be considered orthogonal to any horizontal uncertainty, as stated in the paragraph 3.2.2.1. It should answer two questions. Does the compliance of the suction pad or the contact between the part and the suction pad induce lateral motion? And can the suction pad lift the part without being in contact with it? It doesn't include any manipulation by the robot that would add an uncertainty in position. It has been handled with the first version of the end effector, with the suction pad. The setup of the experiment is shown in Figure 4.3. The end effector is attached to a vertical positioning stage, itself attached to a post mounted on the optical table. The positioning stage is an optical instrument (Edmund optics NT37-956), providing an excellent lateral stiffness. Combined with the contact switch, it also provides a vertical accuracy within a micron. The end effector and the measurement platform are the same as described in sections 3.2.2.1 and 4.1.

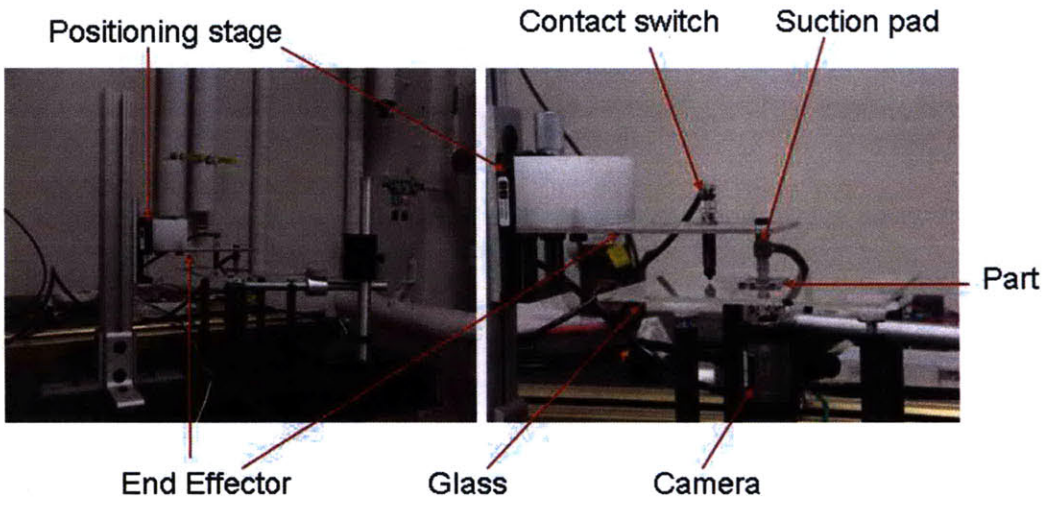

Figure 4.3: Setting of the suction pad experiment
a) global view b) close view

The principle of the experiment is schematized in Figure 4.4. It consists of 7 steps.

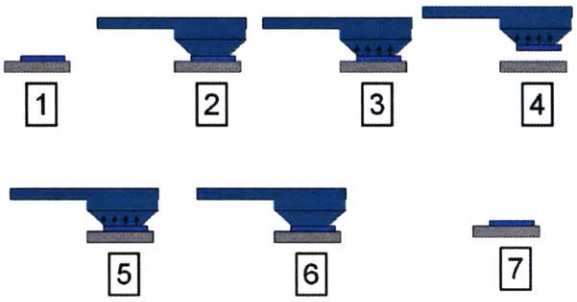

Figure 4.4: Principle of the suction pad experiment

- Step 1: The part is laid on the surface. This is the reference position.
- Step 2: The end effector moves down into contact with the part.
- Step 3: The vacuum is turned on.
- Step 4: The end effector moves up: the part is lifted.

- Step 5: The end effector goes down again at the same vertical position as in Step 2.
- Step 6: The vacuum is turned off
- Step 7: The end effector moves up. The contact with the part is broken

These 7 steps make a cycle that should be repeated many times. It mimes a real pick and place process as it would be done by the robot.

4.2.2 Principle of analysis

The camera takes pictures in all but step 4. The picture of the step 7 of one cycle is the same as the picture of step 1 of the next cycle. The displacement between steps 1 and 7 is the overall displacement due to the lateral variations of the suction tool (contact or friction), as well as to the lateral compliance of the positioning stage. To characterize the repeatability of the suction tool alone, the displacement due to the positioner has to be subtracted from the overall displacement.

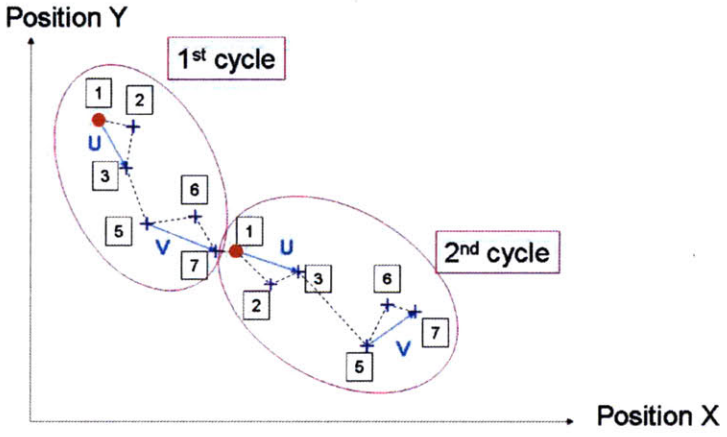

Figure 4.5: Principle of analysis of the suction pad experiment

A schematic example of the positions of the cross in an X-Y plane is shown in Figure 4.5. The vector U represents the change in position between steps 1 and 3, corresponding to the approach of the end effector. Between steps 3 and 5, the part is picked and placed: if the positioner was perfect, the positions at steps 3 and 5 would coincide. Between positions 5 and 7 (vector V), the end effector breaks the contact with the part. The red points correspond to the reference point for each cycle (the first position). Lines are drawn between each point and the next one to show the real-time trajectory of the part.

Thus, the variation induced by the suction tool is characterized by the norm of the sum of the vectors U and V:

$$C=||U+V||$$

4.2.3 Results

For this experiment, 10 cycles have been completed. The positions of the cross for each image taken by the camera are shown in Figure 4.6 in the same format as shown previously. Some positions are so close that they overlap each other on the figure. An overall diagonal trend appears in the trajectory of the part: this is due to a slight non-parallelism between the end effector and the platform; the part is actually slowly sliding on the surface.

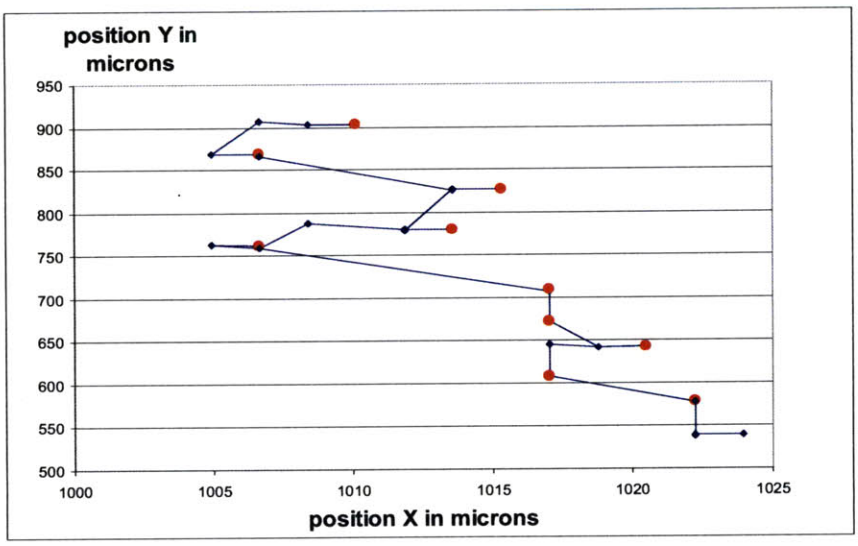

Figure 4.6: Positions of the cross in the suction pad experiment

The displacement is computed for each cycle as explained in section 4.2.2. The results are shown in Figure 4.7: each point corresponds to one cycle. The average displacement for these 10 cycles is 2.89 microns, which is more than 15 times smaller than the horizontal repeatability of the robot. Thus, we conclude that the suction tool doesn't induce any significant lateral displacement: it can be considered orthogonal to horizontal alignment.

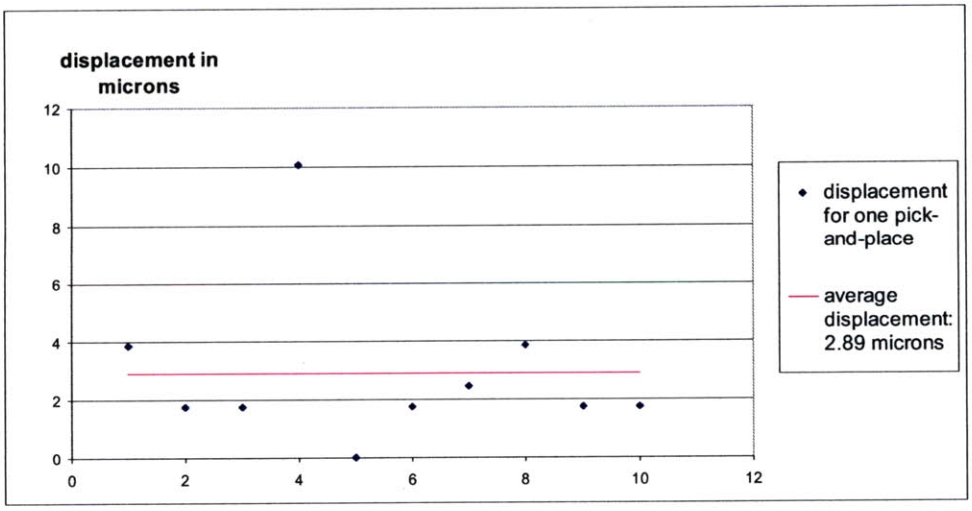

Figure 4.7: Displacement of the part during the suction pad experiment, assuming no variation error induced by the positioning stage

This result confirms *a posteriori* the pertinence of our choice of a suction tool for the handling strategy and its consistence with the choice of a SCARA robot for the large-scale positioning.

4.3 Alignment with vacuum chuck and robot

From now on, the end effector used for the experiments is the second version, - the vacuum chuck as the picking tool and foam walls to achieve the alignment function.

4.3.1 Cycling experiment from one arbitrary point to the aligned position

For this experiment, the goal is to characterize the repeatability of the alignment strategy by itself, by minimizing the number of manipulations and the displacement of a PMMA blank.

The experiment has 3 steps:

- Step 1: The blank is placed in a determined position that is close to the pins, but not in contact with them.
- Step 2: The end effector pushes the blank against the pins; the specifics of this step will be described later.
- Step 3: The blank is picked up, lifted by the vacuum chuck and placed again at the position of the first step.

These 3 steps make a cycle that is repeated many times without any intervention from the experimenter. The camera takes images at the end of the second step.

The step 2 is detailed in Figure 4.8. First, the part lies close but away from the pins (a). Then the end effector pushes the part until contact with the pair of pins: the force should be enough to maintain the contact, but not so large that the part could not move laterally (b). Finally, the end effector pushes the part laterally, against the third pin, while maintaining the part in contact with the pair of pins (c). After that, the end effector steps back and it repeats steps b and c. This repetition comes from the observation that a first alignment would cancel the biggest variations; a second one would achieve the finest positioning.

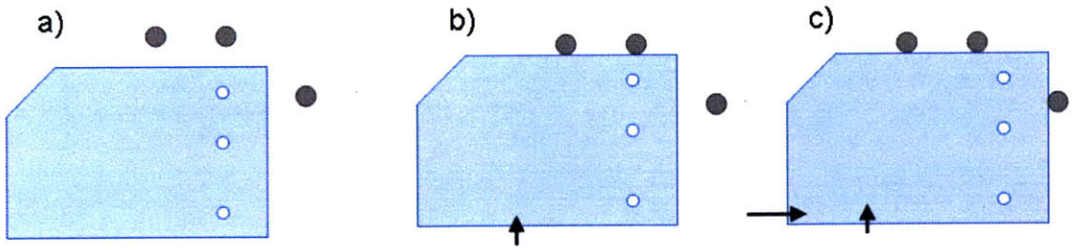

Figure 4.8: Steps of alignment

Figure 4.9 is a figure showing the positions of the blank in an XY plane, computed with the image processing algorithm. The positions are the blue dots. The covariance matrix Σ of the set of data [X,Y] is computed. Then, assuming a normal the probability distribution of the points, the contours of equal probability are ellipsoids centered at the average value of [X,Y] and whose direction and size are governed by the eigenvalues and eigenvectors of Σ (see [25]). We compute then the size of the ellipsoid corresponding to the external contour of an area where the points are with 90% probability. The major radius of this ellipsoid is defined as the repeatability of the set of data.

The magnitude of this repeatability will from now on help us to compare the different conducted experiments. For this experiment, the repeatability is 3.64 microns.

The ellipse corresponding to the contour of the 90% probability area computed from the covariance matrix is drawn in red. Almost all positions lie inside that ellipse, which gives us a good estimation of the uncertainty that we should expect.

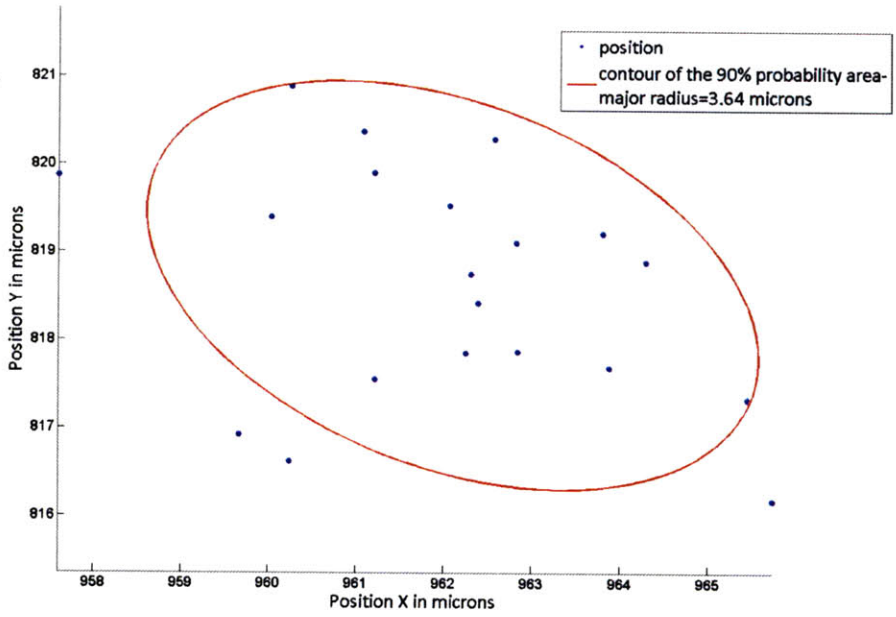

Figure 4.9: Positions of the part in the cyclic alignment experiment

The variation of orientation of the part is also computed: notice that an orientation of 0° corresponds to the orientation of the first image, which means that each orientation is relative to this reference. The results are shown in Figure 4.10. The average orientation is 0.02° and the standard deviation is 0.1°. Notice that the average orientation is smaller than the resolution of the algorithm: nothing can be deduced from this value. However, the standard deviation is significant: we can deduce from this experiment that the orientation varies from about 0.1° around the reference.

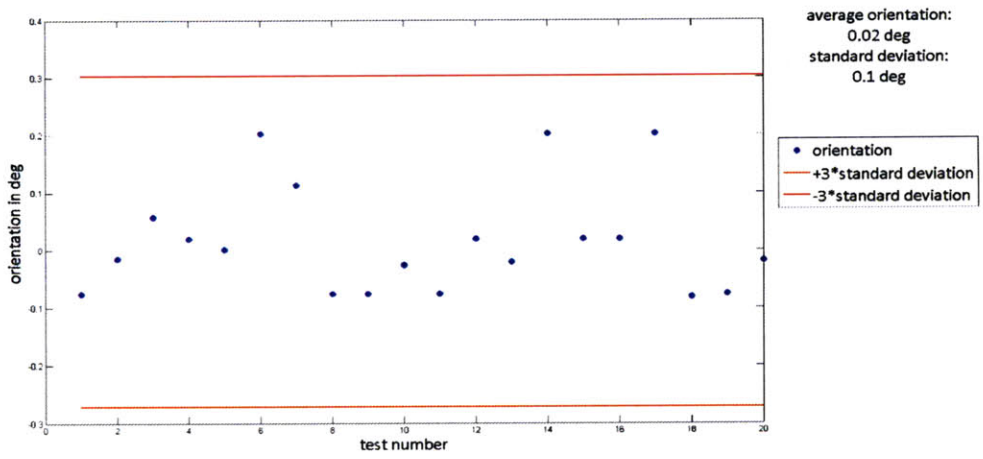

Figure 4.10: Variation of the orientation of the part in the cyclic alignment experiment.

The conclusion of this experiment is that it is possible to align a simple part from a given location with a repeatability of at least 4 microns by using compliant manipulation and a kinematic coupling.

4.3.2 One way experiment from the part feeder to the aligned position

The goal of this experiment is to determine the precision with which we can align a part from an original location subject to variations to a fixed position.

To proceed, the setup will include the part feeder: more details on its role and its design can be found in Chapter 5, but we can already say that it is supposed to be the station where the blanks are stacked at the beginning of the assembly. The part feeder stores the blanks and theoretically presents them to the robot always at the same location. In reality, the design is not perfect, which means that this position is subject to variations that are larger than the repeatability of the robot.

Unfortunately, it is easy for the robot to pick a part from the part feeder, but the latter can only be manually loaded. This means that this experiment can not be fully automated and has to include an intervention from the experimenter. A cycle consists of 3 steps:

- Step 1: The robot picks a part from the part feeder and places it close to, but not in contact with, the pins.
- Step 2: The end effector aligns the part against the pins.
- Step 3: The experimenter takes the part and places it back in the part feeder.

The camera takes an image at the end of the second step. The results are presented as previously in Figure 4.11 and Figure 4.12.

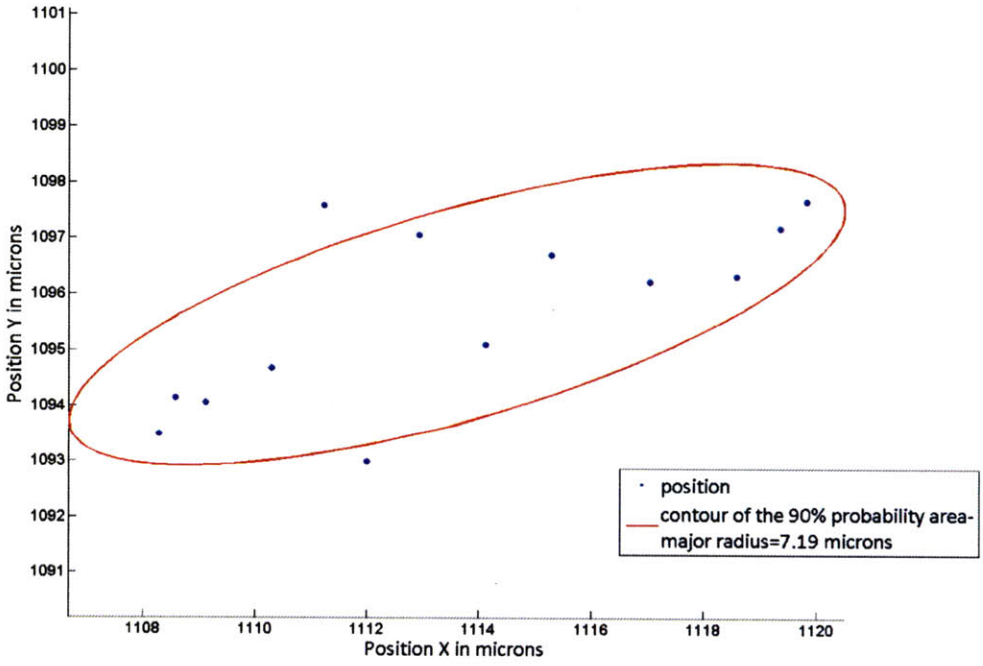

Figure 4.11: Positions of the part in the one-way alignment from the part feeder experiment.

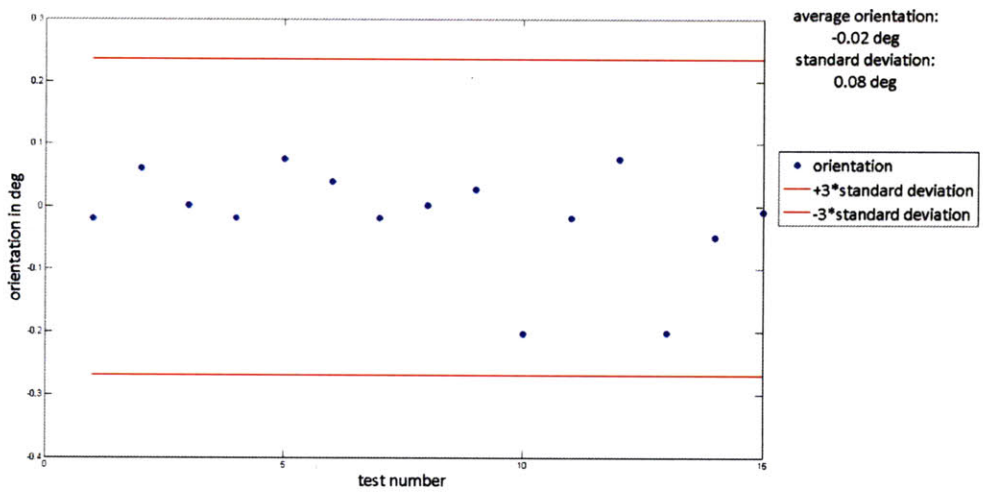

Figure 4.12: Variation of the orientation of the part in the one-way alignment from the part feeder experiment.

The position repeatability characteristic of this experiment is 7.19 microns. Since the resolution of the algorithm is 1.75 microns, this value is known with an uncertainty of ±1.75 microns. The same thing happens to the repeatability characteristic of the cyclic alignment experiment (3.64 microns). If these values differ of less than two times the resolution of the algorithm, they must be considered equal. This is the case here:

$$||\ 7.19\pm1.75\ |-|\ 3.64\pm1.75\ || = 0.05$$

We conclude that both experiments have the same position repeatability. The variation of orientation has also the same magnitude as the previous experiment.

Thus, the alignment strategy is robust to variations in the original position that are larger than the position repeatability of the robot. These variations will be characterized later in Chapter 5.

4.4 Alignment on two platforms

4.4.1 Alignment on both platforms

The alignment takes place in different stations located at different places in the work area of the robot. Theoretically, the repeatability of the robot is not constant in the entire workspace. One of the purposes of the alignment strategy is to cancel this variation. On the other hand, the set of three pins that we use for the kinematic coupling can not be identically (with a micron accuracy) replicated in two different stations. As such, the alignment should not depend on the way these three pins are arranged.

In this experiment, the goal is to determine if the repeatability of alignment strategy depends on the shape and position of the kinematic coupling.

To proceed, two different inspection platforms have been used. One cycle consists in four steps:

- Step 1: The part is aligned on platform 1 against the pins.
- Step 2: The part is picked up from platform 1 and placed on platform 2.
- Step 3: The part is aligned on platform 2 against the pins.
- Step 4: The part is picked up from platform 2 and placed on platform 1.

The cameras take images at the end of Step 1 and Step 3. The computed positions are shown in Figure 4.13. The repeatability characteristic of the alignment on each platform is 4.07 microns for platform 1 and 4.45 microns for platform 2. The difference of these two values is less than the resolution of the image processing algorithm, which means that they can be considered equal.

The variation of orientation on each platform is equivalent.

We can conclude that the alignment doesn't depend on the location where it takes place in the work area of the robot, nor on the arrangement of the three pins- the form of the kinematic coupling. This means that this strategy is robust to displacements, and that the disposition of the set of 3 pins has to be similar in different stations, but not identical within a micron range.

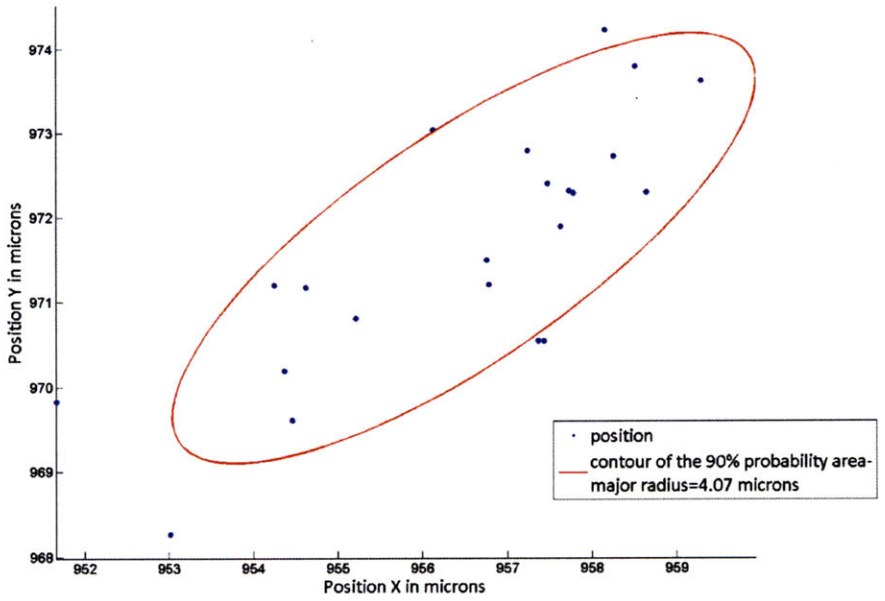

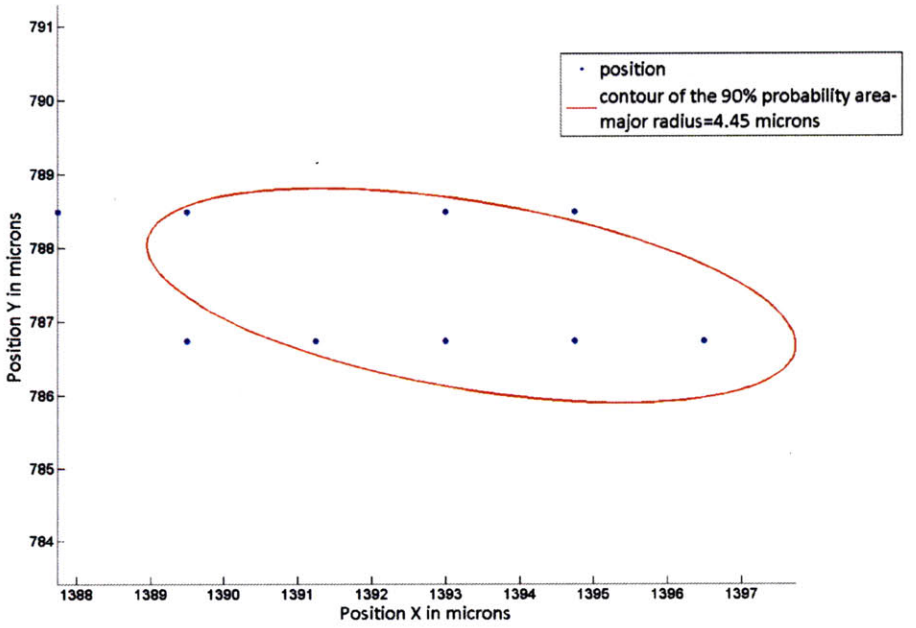

Figure 4.13: Positions of the part in the experiment of alignment on 2 platforms.
a): platform1-b): platform 2

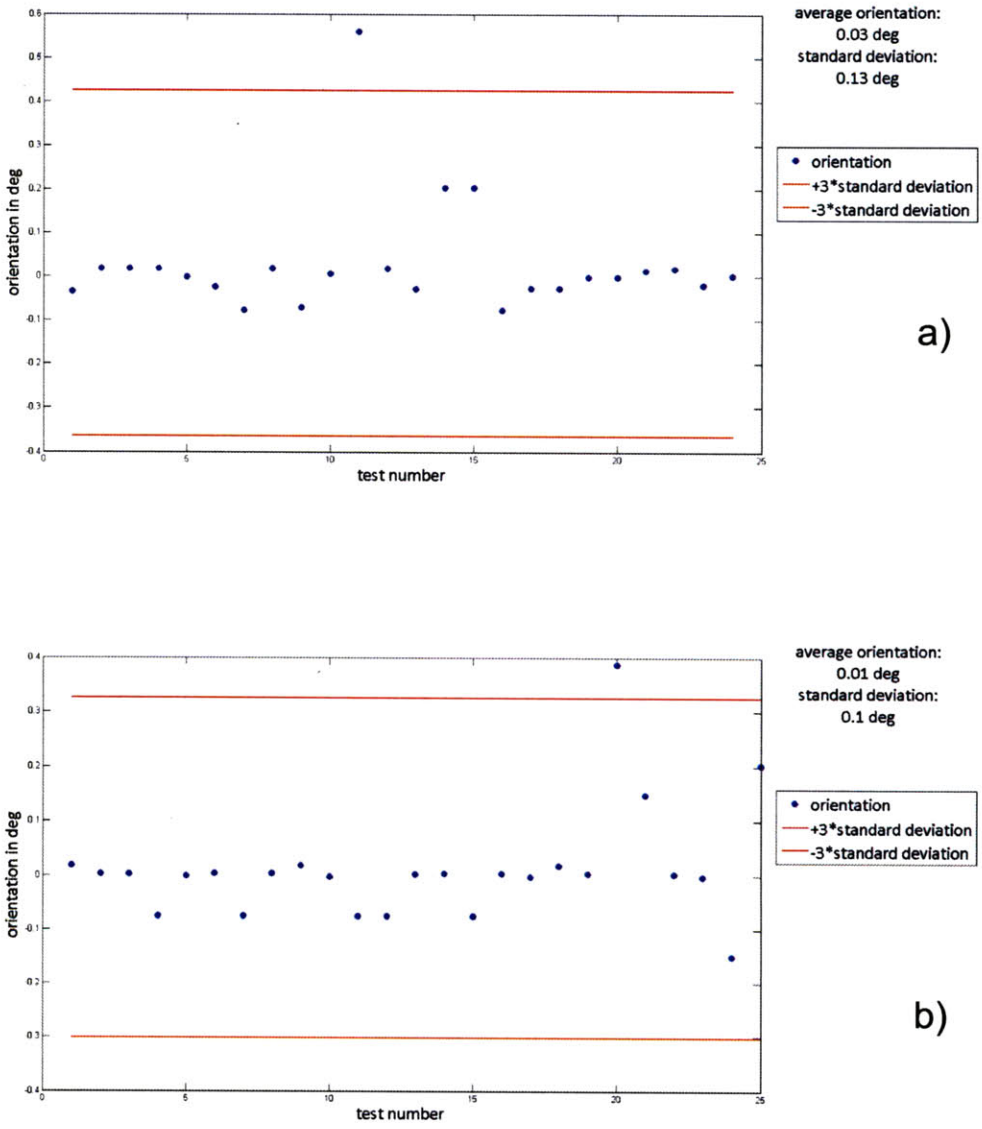

Figure 4.14: Variation of the orientation of the part in the experiment of alignment on 2 platforms.
a): platform1-b): platform 2

4.4.2 Alignment on only one platform: horizontal repeatability of the robot.

Now that it has been proven that the alignment strategy works with a repeatability of about 5 microns, it is possible to determine how this strategy improves the repeatability of positioning of the robot combined with the suction function of the end effector. One cycle of the experiment consists of 3 steps:

- Step 1: The part is aligned on platform 2.
- Step 2: The part is picked up from platform 2 and placed on platform 1.
- Step 3: The part is picked up from platform 1 and placed on platform 2.

The camera takes an image at the end of Step 2. This experiment has also been conducted with an alignment on platform 1 instead of platform 2.

For the repeatability on platform 1, the computed positions are shown in Figure 4.15 and the variation of orientation is shown in Figure 4.16.

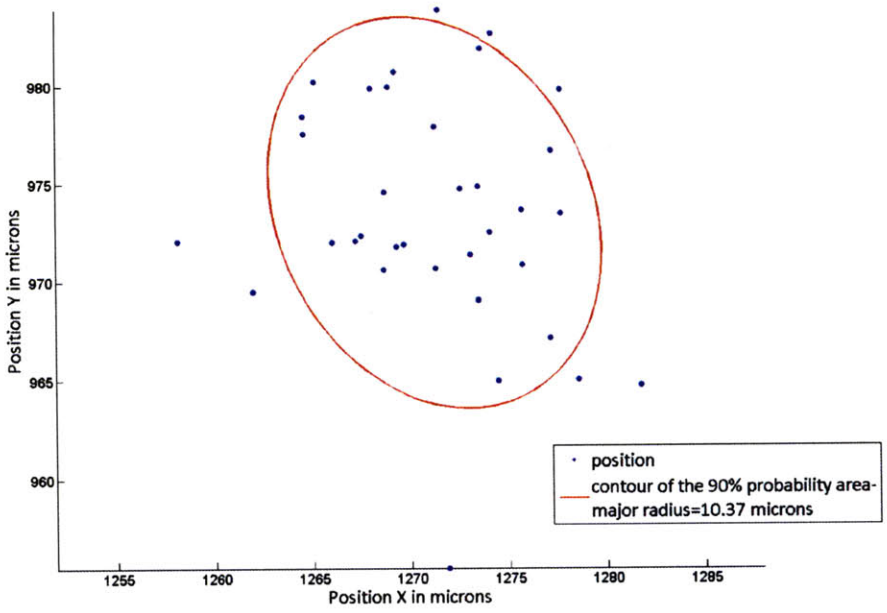

Figure 4.15: Positions of the part in the experiment to determine the repeatability of the robot in platform 1.

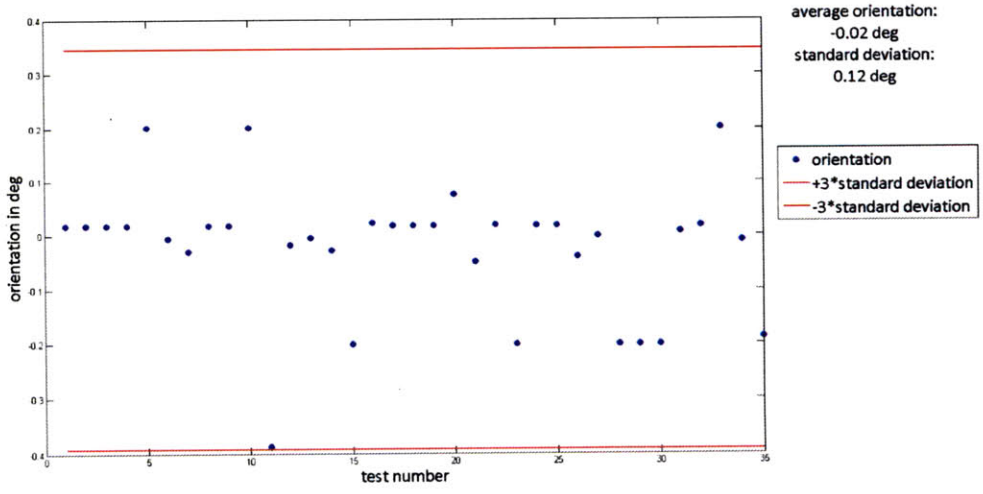

Figure 4.16: Variation of the orientation of the part in the experiment to determine the repeatability of the robot in platform 1.

The same results are shown for the repeatability on platform 2 in Figure 4.17 and Figure 4.18.

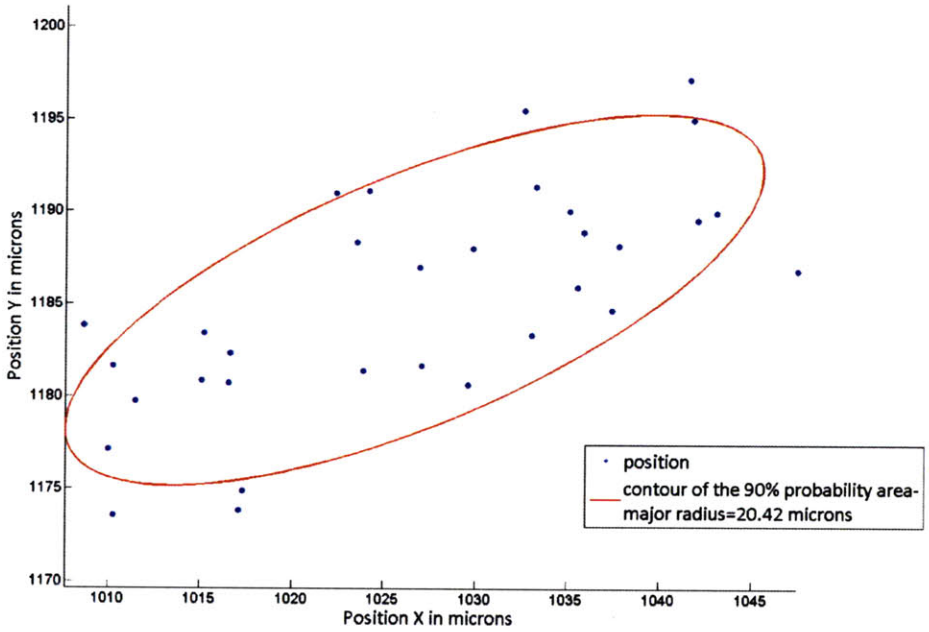

Figure 4.17: Positions of the part in the experiment to determine the repeatability of the robot in platform 2.

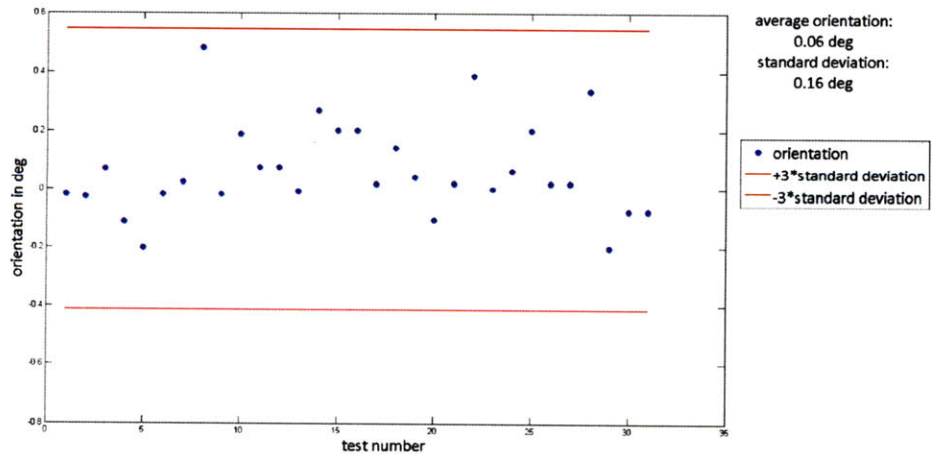

Figure 4.18: Variation of the orientation of the part in the experiment to determine the repeatability of the robot in platform 2.

Since the position of the part when it has been aligned is known with an uncertainty of 5 microns, the variation of position in the non-aligned position is only due to the robot and the end effector, and more precisely the suction tool of the end effector. The error due to the suction tool has already been determined in the section 4.2 and has been shown to be less than 3 microns. Thus, the error during the positioning by the robot on platform 1, whose value is 10.37 microns, is mostly due to the robot, and not the suction tool. The same conclusion stands for the error in position on platform 2 (20.42 microns). As for the orientation, we can not conclude anything from the variations computed from these experiments for the same reasons stated in section 4.3.1.

We can conclude that the repeatability in positioning of the robot that we observed is consistent with the specifications of the manufacturer. As expected, this repeatability depends on the position in the workspace. Furthermore, we proved that the alignment strategy actually cancels these variations.

4.5 Alignment of an embossed part

All the experiments until this point have been conducted with a blank part, but the real alignment should occur after the embossing process which creates a corner that is supposed to be kinematically coupled with the three pins. Thus, to characterize the alignment strategy in a real situation, it should be tested with a previously embossed part.

4.5.1 Alignment against three pins

The experiment was first conducted by aligning the embossed corner against the set of three pins that were previously used. A cycle consists of 3 steps:

- Step 1: The embossed part is picked up from the work area of the hot embossing machine and placed on the platform.
- Step 2: The part is aligned against the pins
- Step 3: The part is placed on the work area of the HEM by the experimenter.

Notice that it is tricky for the robot to place back an embossed part on the work area of the hot embossing machine when the part is still warm. This has to be manually loaded. Indeed, after the embossing process, the part is slightly warped and can be stuck under the fingers used to maintain it during the demolding. Thus, it can be slid out of the fingers but the manipulation has to be really precise to properly place it again. To simplify the experiment, a manual load is sufficient.

The camera takes an image at the end of the step 2. Note that to use the image processing algorithm, the usual detail of a cross drawn on a layer of blue varnish could not be used, but rather one of the fiducials embossed on the microfluidic part. This detail is shown in Figure 4.19.

The positions of this fiducial are shown in Figure 4.20 and the variation of its orientation is in Figure 4.21. The position repeatability is about 11.32 microns, a value twice as large as the

equivalent repeatability for a non-embossed part, but 2.5 times smaller than the repeatability of the robot by itself.

We conclude that the alignment strategy is efficient in a real situation, and can be used for our manipulation.

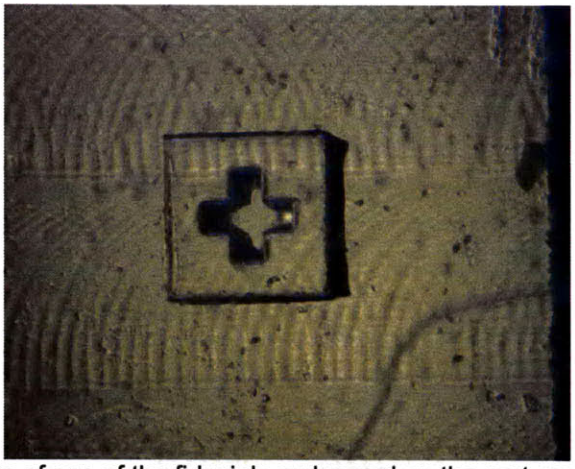

Figure 4.19: Image of one of the fiducials embossed on the part, used to detect the position of the part.

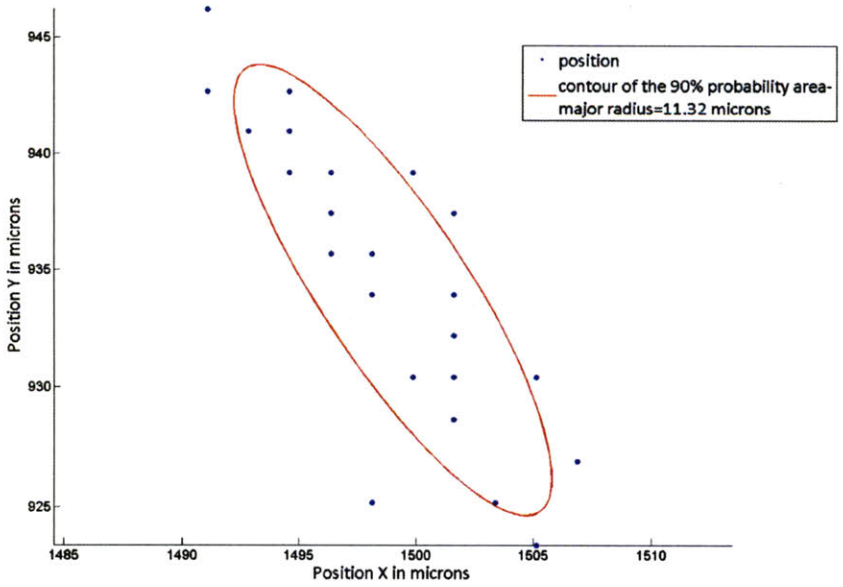

Figure 4.20: Positions of the part in the alignment of an embossed part against 3 pins.

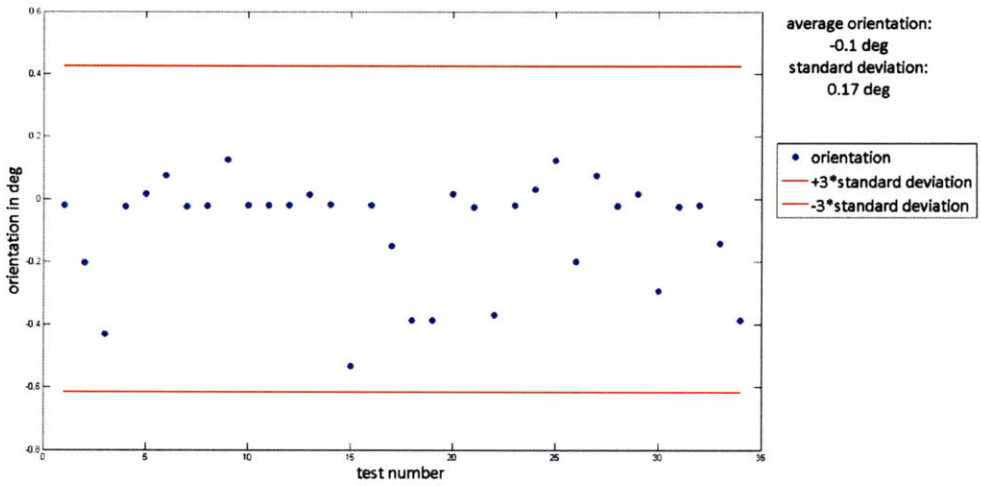

Figure 4.21: Variation of the orientation of an embossed part against 3 pins.

4.5.2 Alignment against a corner

The theory states that three pins are necessary and sufficient to kinematically align the part, but a corner similar to the one used in the hot embossing machine would be easier to machine and less fragile than three pins. If the alignment could work with a corner similar to that corner as well as with the set of three pins, then many machining issues would be avoided. The goal of this experiment is to determine if this alignment would work well enough. Apart from the change of aligner, this experiment is the same as that described in section 4.5.1.

The results of this experiment are shown in Figure 4.22 and Figure 4.23. The repeatability of the position is 35.26, which is about 4 times more than the repeatability of the alignment against the three pins.

We conclude that a corner can not be used in the alignment strategy, even if it is really similar to the corner used to create the corner to align. Actually, the theory states that the more similar the corners are, the more over constrained the coupling between the part and the alignment corner will be, and the worst the alignment will be.

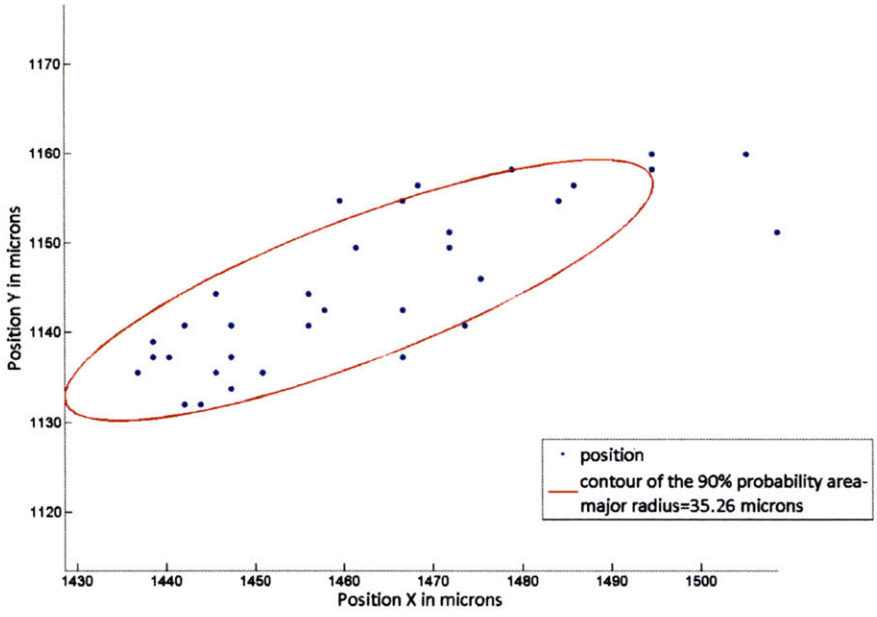

Figure 4.22: Positions of the part in the alignment of an embossed part against a corner

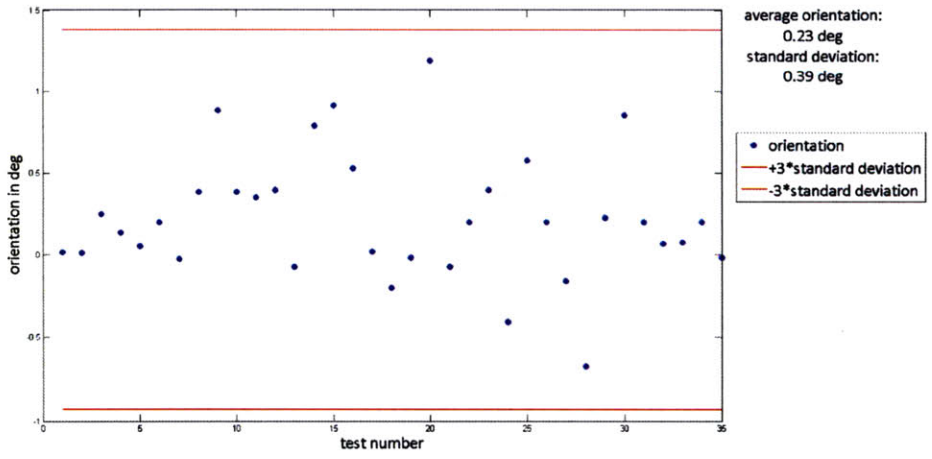

Figure 4.23: Variation of the orientation of an embossed part against a corner.

4.6 Probability distributions of the position

Once the efficiency of the alignment has been demonstrated, it is necessary to better understand the characteristics of the repeatability in position and how these characteristics evolve.

A long-run experiment (250 cycles) has been conducted: the steps are the same as for the experiment that tested the alignment on two platforms (4.4.1). In this experiment though, two images are taken by the camera: one at the end of step 2 (before alignment) and the second at the end of step 3 (after alignment). The positions of the cross on the set of first images are computed and gathered to analyze the repeatability of the robot. The positions on the second images determine the alignment repeatability.

To characterize the repeatability of the positions, the vectors X and Y are analyzed. It is necessary to know what their probability distribution is. Only the most classical distributions will be considered, since their physical interpretation is the most obvious.

First notice that the vectors that we call X and Y are arbitrary: these directions are dictated by the relative orientation of the camera and the cross, which doesn't have any physical meaning. The only real meaning is the position in the plane. Thus, a rotation of X and Y in the plane won't affect the characteristics of the positions. This is particularly useful to decouple the analysis of these two sets of data. Indeed, it is more difficult to recognize a normal or uniform distribution in two dimensions than a bell shape or a flat segment. That's why the [X,Y] matrix should be rotated to cancel the correlation between X and Y. To do so, the covariance matrix Σ is computed. If Σ is not diagonal (and there is no reason why it would be diagonal), the matrix R formed by its normalized eigenvectors is computed: R is a rotation. This rotation is applied to [X,Y] and gives two new sets of data: X_{rot} and Y_{rot}. Then the covariance matrix of X_{rot} and Y_{rot} is diagonal, which means that these vectors are decoupled.

4.6.1 Robot

After rotation of the positions X and Y for the first set of data, the rotated positions are separately plotted in histograms where the width of each bar is the size of a pixel, and the central bar is centered on the mean of the set of data. These plots are shown in Figure 4.24 and Figure 4.25. It is almost obvious that it is a normal distribution: to confirm this assumption, an approximated normal probability density function corresponding to the same means and standard deviations as the vector and normalized to fit the histogram is plotted along with the histogram.

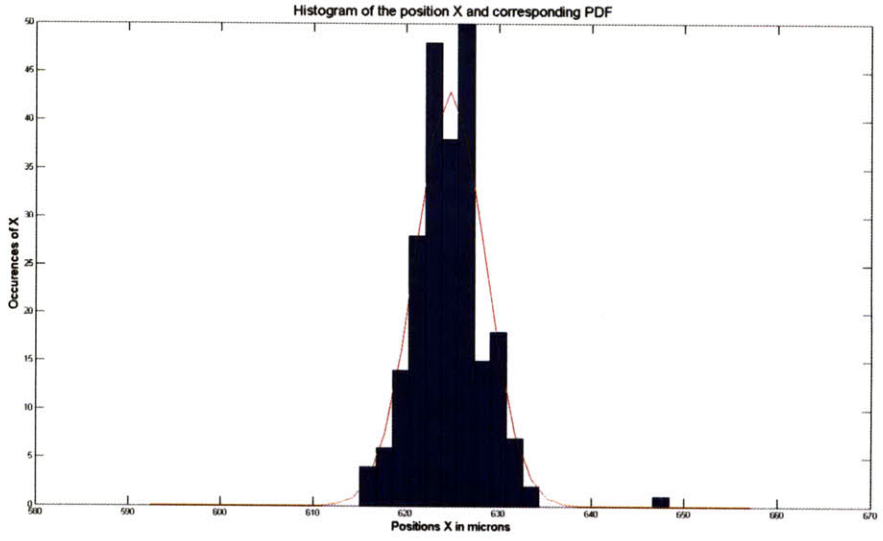

Figure 4.24: Histogram of the positions X for the repeatability of the robot.

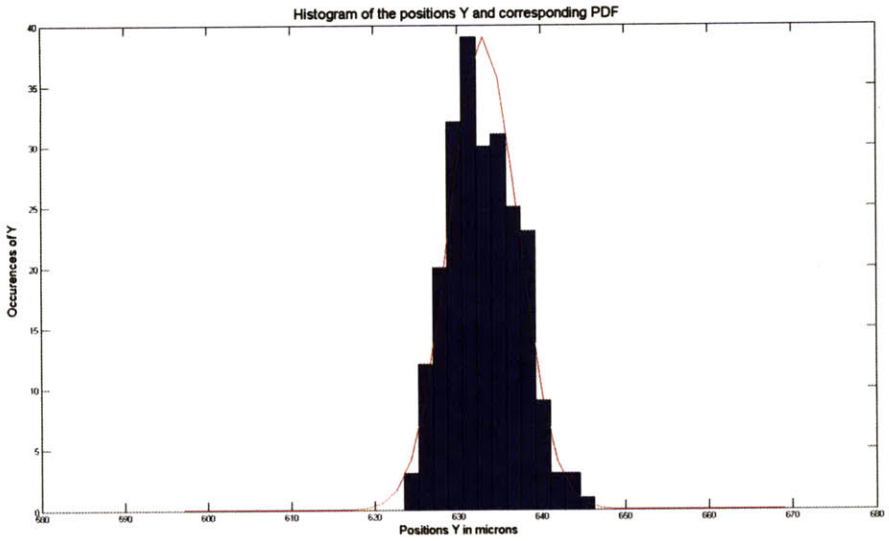

Figure 4.25: Histogram of the positions Y for the repeatability of the robot.

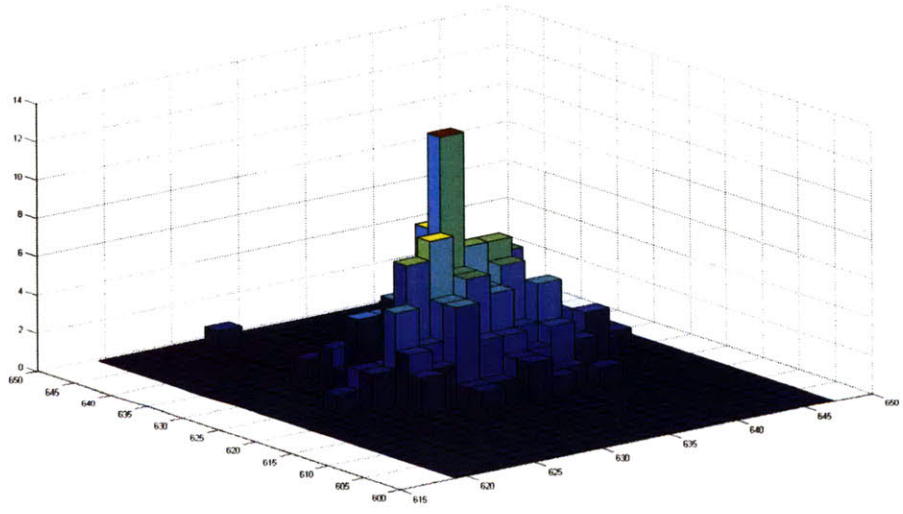

Figure 4.26: Histogram in three dimensions of the positions X and Y for the repeatability of the robot.

A histogram in three dimensions to see both X and Y is also plotted in Figure 4.26. We can conclude from this quick study that the probability distribution of the positions characteristic of

the robot is normal, or purely random. This means that no physical effect occurs that might make the repeatability get worse: this repeatability is the best that we could get from the robot.

4.6.2 Alignment strategy

The same analysis is done for the second set of positions, corresponding to the repeatability of the alignment strategy.

The histograms of X_{rot} and Y_{rot} are plotted in Figure 4.27 and Figure 4.28 along with the corresponding normal probability density functions. The nature of the probability distribution is less obvious in that case. The vector X seems normal, but Y has two peaks of probability, instead of one. Physically, it could mean that the part has two preferred positions and can randomly go to one or the other, maybe because of friction: if the force doesn't overcome this friction, the part stays in one position, but if it does, the part goes to the other position. It might mean that the alignment could be improved. However, it is already enough for the requirements of this part.

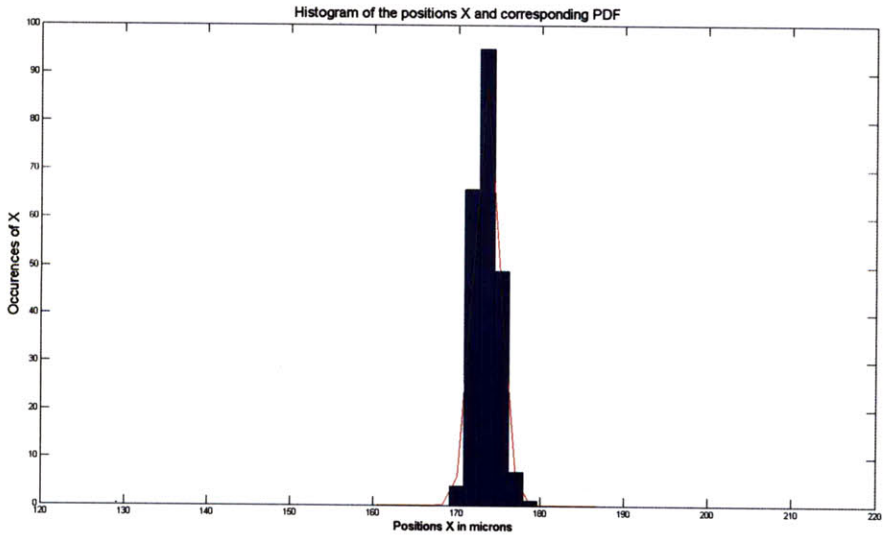

Figure 4.27: Histogram of the positions X for the repeatability of the alignment strategy.

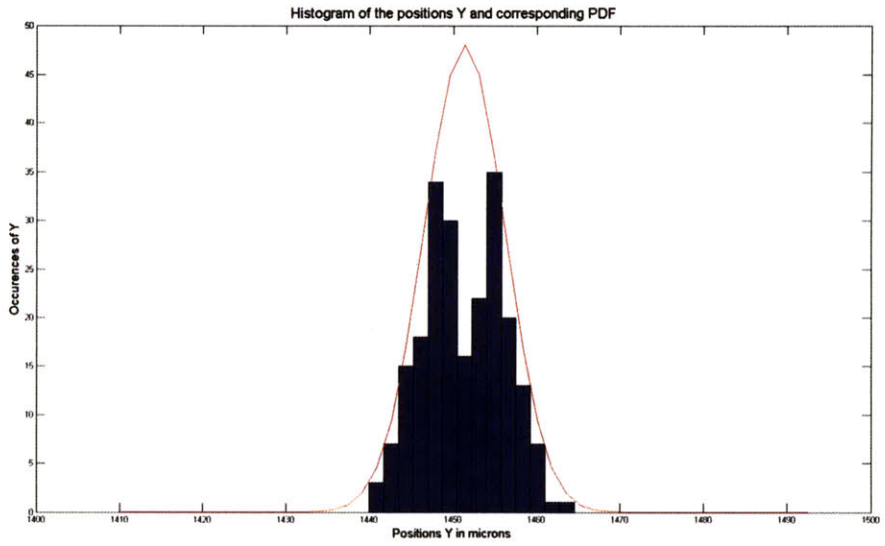

Figure 4.28: Histogram of the positions Y for the repeatability of the alignment strategy.

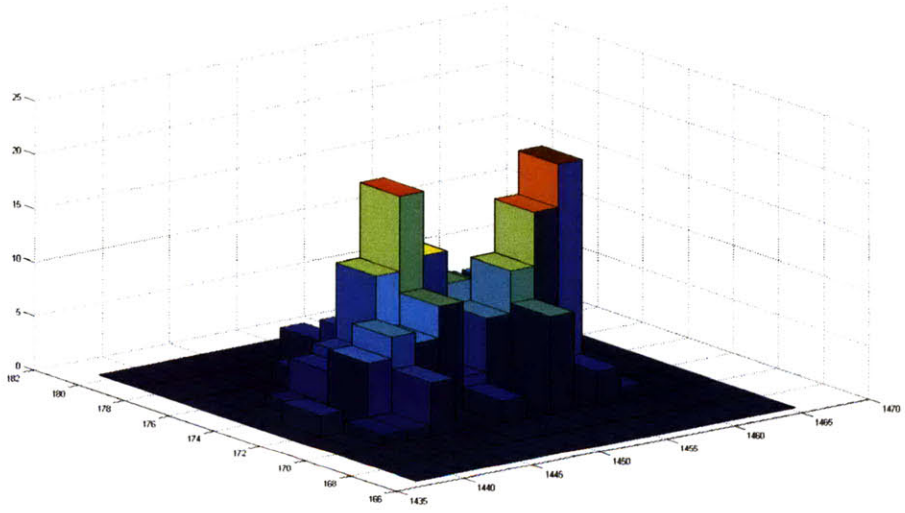

Figure 4.29: Histogram in three dimensions of the positions X and Y for the repeatability of the alignment strategy.

4.7 Summary of the position repeatability results

To conclude this chapter, a table summarizing the repeatability results is included in Table 6.

Experiment	Position repeatability in microns
Repeatability of the Suction tool (4.2)	2.89
Alignment from an arbitrary point (4.3.1)	3.64
Alignment from the part feeder (4.3.2)	7.19
Alignment on platform 1 (4.4.1)	4.07
Alignment on platform 2 (4.4.1)	4.45
Repeatability of the robot on platform 1 (4.4.2)	10.37
Repeatability of the robot on platform 2 (4.4.2)	20.42
Alignment of an embossed part against 3 pins (4.5.1)	11.32
Alignment of an embossed part against a corner (4.5.2)	35.26

Table 6: Summary of the repeatability results presented in Chapter 4.

Chapter 5.

First position: the part feeder

5.1 Design

As mentioned in paragraph 4.3.2, the part feeder is the first station of the production cell. It is meant to store about 50 parts, and to consistently present them to the robot in the same position. To design this component, the horizontal and vertical positioning were decoupled.

The vertical alignment is achieved through the combination of a spring loaded platform and a flange. The stack of parts is laid between a plate and a flange; the plate is attached to the flange by extension constant force springs. The plate can move vertically in the box, but the flange is rigidly mounted on the box. So, regardless of the height of the pile of parts, it is always pushed against the flange with the same load, and the part on the top is always at the same level in the box. This greatly simplifies the programming of the assembly: the program doesn't have to take into account how many parts are left in the box, it merely picks up the top part, which is always in same position, until the part feeder is empty.

The horizontal alignment is inspired by the corner + three pins arrangement described in section 3.1.3 for alignment on the embossing stage. Three fine rods are placed inside the box, as shown in Figure 5.1.c. Just before picking up a part, the end effector, using its alignment function, pushes the part against the rods. Foam, combined with frictionless Teflon tape, is used to keep the lower parts as close as possible to these rods.

Finally, the strategy to take the part out of the box consists of 4 steps:

- Step 1: the end effector aligns the top part against the rods.

- Step 2: the end effector moves to the pick position, and pushes the pile of parts low enough to make sure that the upper part doesn't touch the flange anymore.
- Step 3: the vacuum is switched on, and the upper part is slid out of the box. It isn't in contact with the flange so it isn't damaged. The second part is help in the part feeder by a front wall whose height is designed to be between the bottom faces of the upper and second parts.
- Step 4: the end effector moves up. The second part is now the top part.

A 3D representation of the part feeder is shown in Figure 5.1 along with some detailed views. Notice that the springs used in this representation are regular extension springs instead of the constant force extension springs used for the realization of the part feeder. Figure 5.1.a shows a global view of the part feeder. The flange consists of two plates mounted at the top of the box. The fine rods are shown in red and the parts are in transparent blue. In Figure 5.1.b, a close view shows better details about the way how the parts are pushed against the flange by the spring loaded platform. Finally, Figure 5.1.c is a top view where one half of the flange has been made transparent to show the alignment of the parts against the rods.

The realization of the part feeder is in Figure 5.2.

Notice that the part feeder is the first station of the production cell, and thus is intended to be manually loaded.

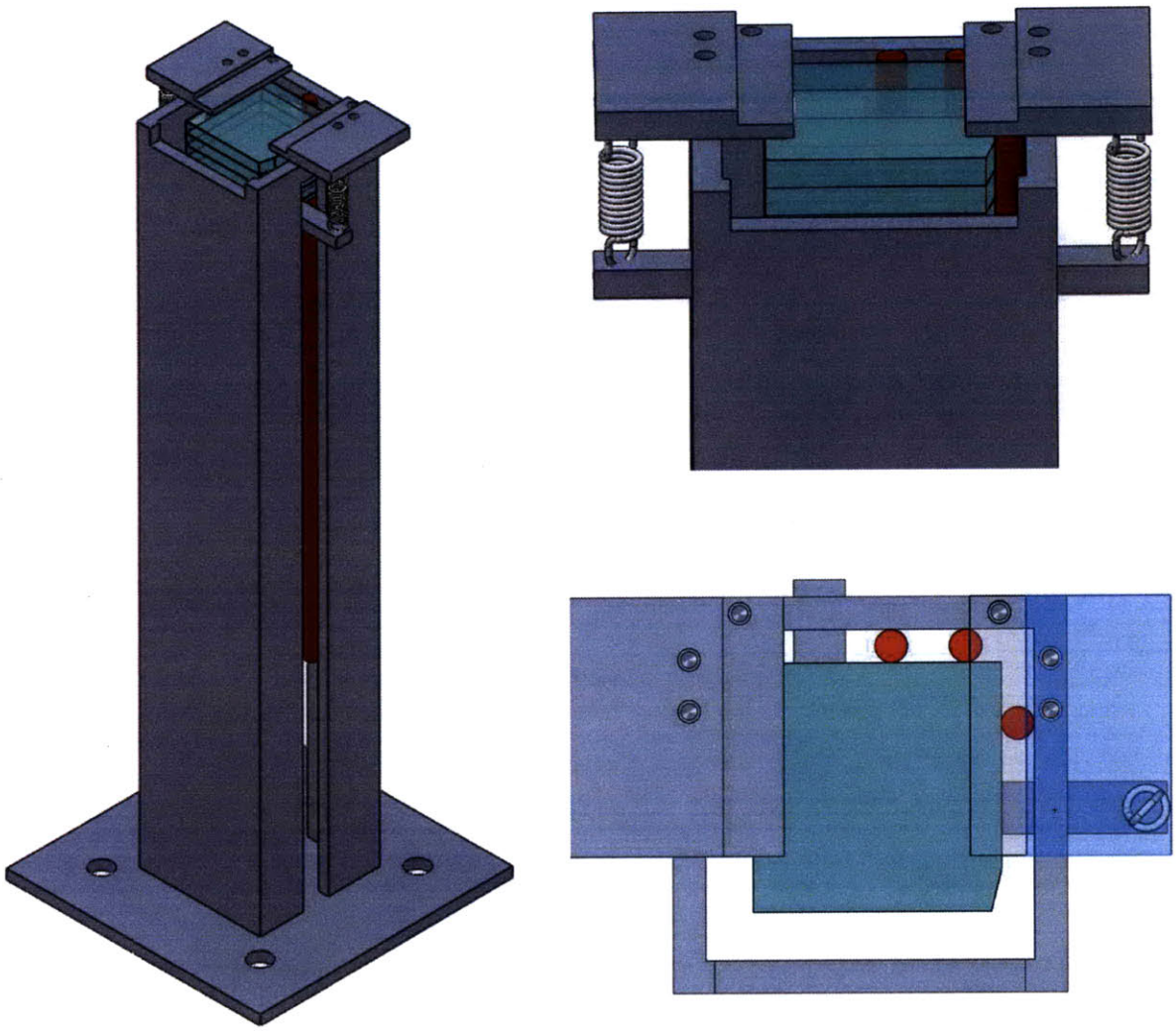

Figure 5.1:3D representations of the part feeder
a: global view- b: close view of the spring loaded platform- c: horizontal alignment of the parts

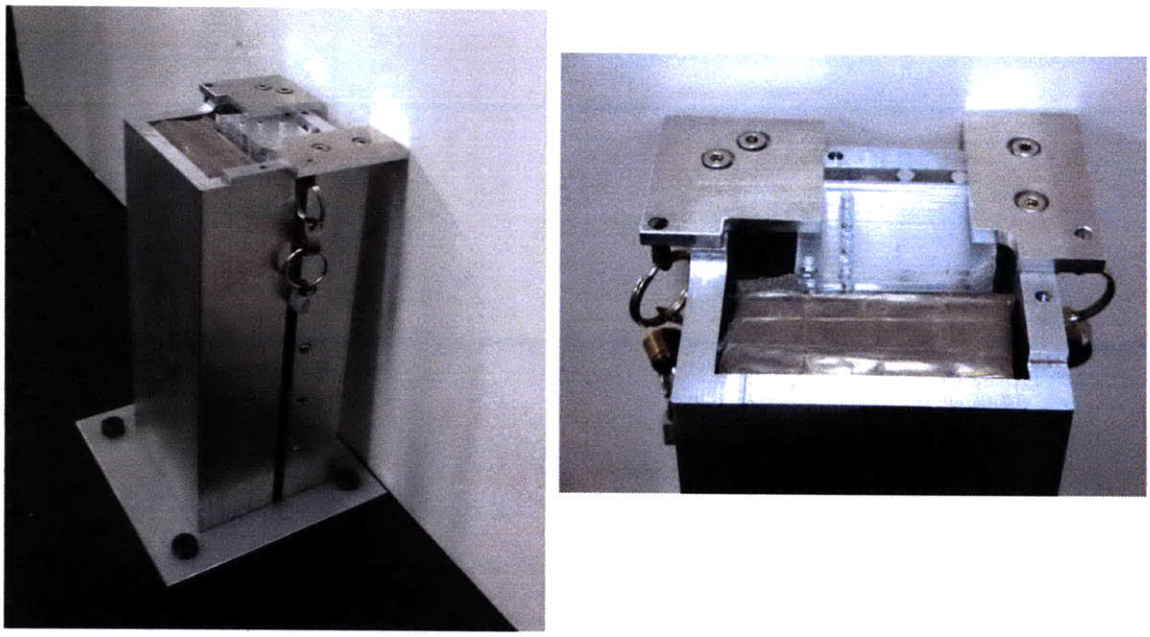

Figure 5.2: Realization of the part feeder

5.2 Repeatability of the part feeder

An experiment has been conducted to determine the repeatability of the position of the upper part in the part feeder; this is to say its efficiency. It consists of 3 steps:

- Step 1: the upper part is slid out of the part feeder following the steps detailed in paragraph 5.1.
- Step 2: the part is placed on an inspection platform. No alignment is performed.
- Step 3: the part is manually loaded by the experimenter back into the top position of the part feeder.

The camera takes an image at the end of Step 2. The resulting positions of the part are shown in Figure 5.3, and the variation of its orientation in Figure 5.4.

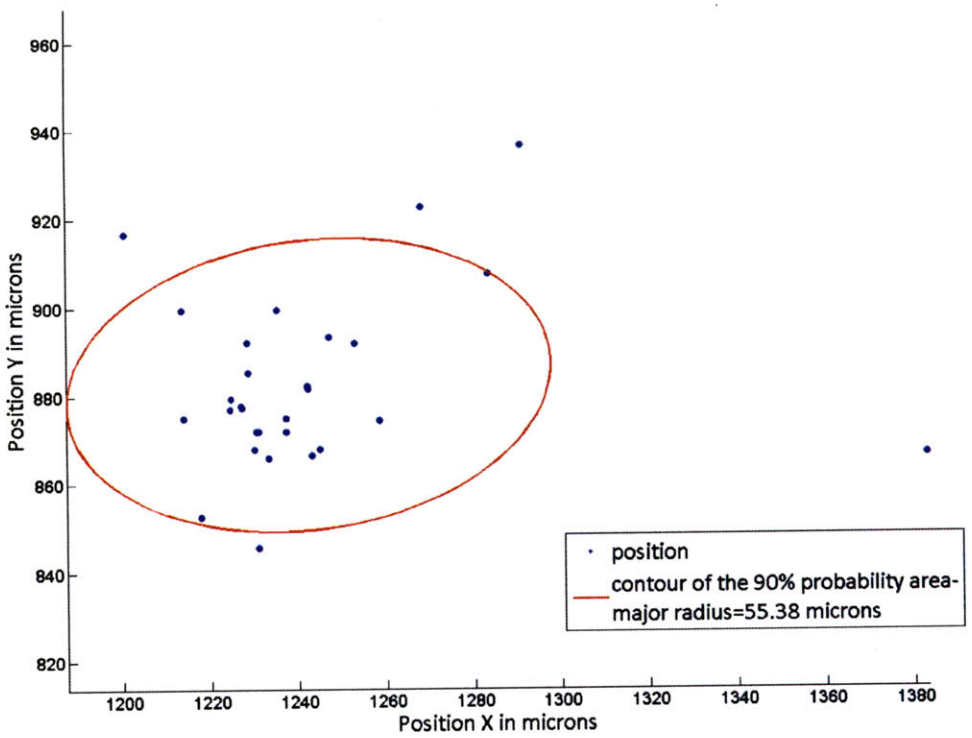

Figure 5.3: Positions of the part in the experiment to determine the repeatability of the part feeder.

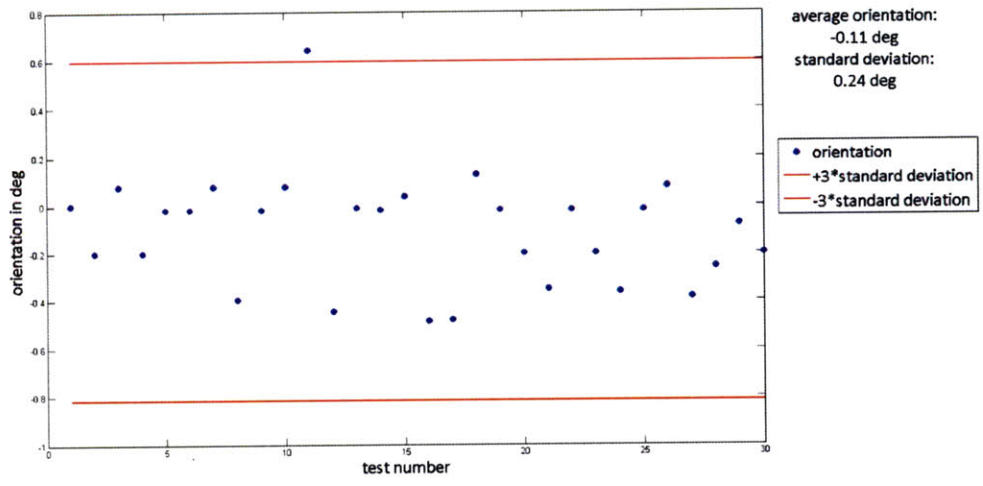

Figure 5.4: Variation of the orientation of the part in the experiment to determine the repeatability of the part feeder.

This experiment has been conducted for different sizes of stacks in the part feeder, to make sure that any part can be picked up from it with the same repeatability in position. The results of these experiments were all equivalent: the repeatability in position is about 50 microns, which is twice as large as the repeatability of the robot as determined in section 4.4.2. This means that the error in position is characteristic of the part feeder itself. This value is large compared to the repeatability of the robot, but remember that this is only a mechanical alignment: it couldn't be as good as the positioning of an arm finely controlled by the use of precise sensors. Moreover, it has been proved in section 4.3.2 that the alignment strategy can overcome this error and divide it by more than 6.

The conclusion of this experiment is that the part feeder doesn't provide a perfect original position of the part in the production cell, but its positioning is accurate enough for our manipulation.

Chapter 6.

Implementation on the other machines and analysis of the results

Once the alignment strategy was demonstrated to be effective by itself, it could be integrated to the complete manipulation and tested. To achieve a full automation of the production, a communication network was created, allowing the substations to share information with the master controller, which is the controller of the robot. First, a simple cycle was implemented to achieve embossing and inspection; then bonding was added.

6.1 Communication

As explained in 1.2.2, the manipulation must be coordinated by one master controller: we chose the controller of the robot to play that role. Since the manipulator has to step in before and after each process, it makes sense to let it call the tune. Moreover, the multiple available inputs and outputs of the controller make the setup of a communication network easier.

This communication consists of both inputs and outputs between the controller and each station (from the controller view point):

- The outputs from the controller to the station are:
  - ✓ Begin task;
  - ✓ Substrate has been removed from the station;
  - ✓ Error.
- The inputs from the station to the controller are:

- ✓ Ready to begin the task;
- ✓ Task is finished;
- ✓ Error.

Notice that the errors can be transmitted both from and to a station: since two stations can not communicate directly with each other, it is necessary to allow them to share some information through the controller.

Once this network is installed, the manipulation is programmed based on the following scenario:

- In the initial state, the outputs from the controller are off;
- Wait for the input "Ready to begin the task";
- *Place the substrate in the station;
- Send the output: "Begin task";
- Wait for the input "Task is finished";
- *Remove the substrate from the station;
- Send the output: "Substrate has been removed from the station";

The steps related to manipulation to and from a specific station (preceded by a star *) are subject to additional conditions due to the presence of other stations before and after this one. For example, the substrate can not be taken to bonding if inspection is not finished. Details about the overall manipulation to maximize the throughput of the production cell are given in Chapter 7.

6.2 Simple cycle: embossing and inspection

In this first try to fully automate the production of the fluid mixer, only the embossing and the first inspection stages are integrated.

The operations are as follows:

- The substrate blank is picked up from the part feeder.

- The blank is positioned and registered in the hot micro embossing machine (HME). The HME cycle is executed.
- The part is positioned and registered in the inspection stage, and inspected. At this point, the inspection stage is the measurement platform described in 4.1. An image of a fiducial (a Swiss flag) is taken.
- The part is placed in a Petri dish.

Several cycles are achieved and the positions of the cross in the image are computed. These positions are plotted in Figure 6.1 and the variations of the orientation are plotted in Figure 6.2. As explained in 3.1.3, if the corner was perfectly replicated during the embossing, the position of the cross with respect to the corner should be exactly as repeatable as the position of the upper platen (the embossing tool) with respect to the master corner of the embossing machine.

The repeatability results (more than 200 μm in position and 1° in orientation) suggest that another source of uncertainty hides in this data.

Actually, an imprecision is observed during the embossing: while the upper platen applies a pressure on the middle part of the substrate, the sides not submitted to this pressure slightly warp and curve up: as a consequence they don't touch one of the sides of the corner (see Figure 6.3). Thus, this side of the corner is not created in the part and the alignment depends on the shape of the edge cut by the laser. This edge has a rough texture that strongly varies from one part to another and the position repeatability in the direction orthogonal to that edge is degraded by this variation. Notice that the ellipse defining the contour of the 90% probability area is very long: its major radius is more than two times larger than the minor radius. This means that the position uncertainty is strongly related to one direction: after verification, we realized that the major axis of this ellipse is orthogonal to the edge of the part where the corner has not been created, which confirms the previous explanation.

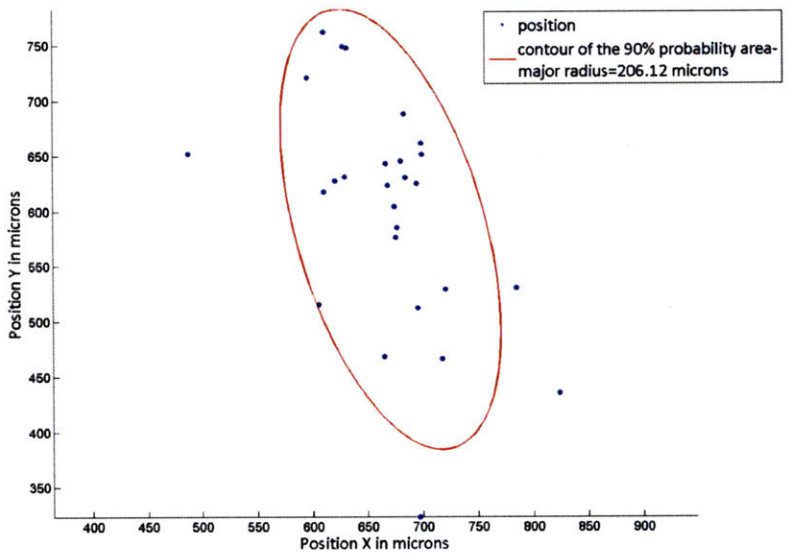

Figure 6.1: Positions of the part in the experiment to determine the repeatability of the simple cycle.

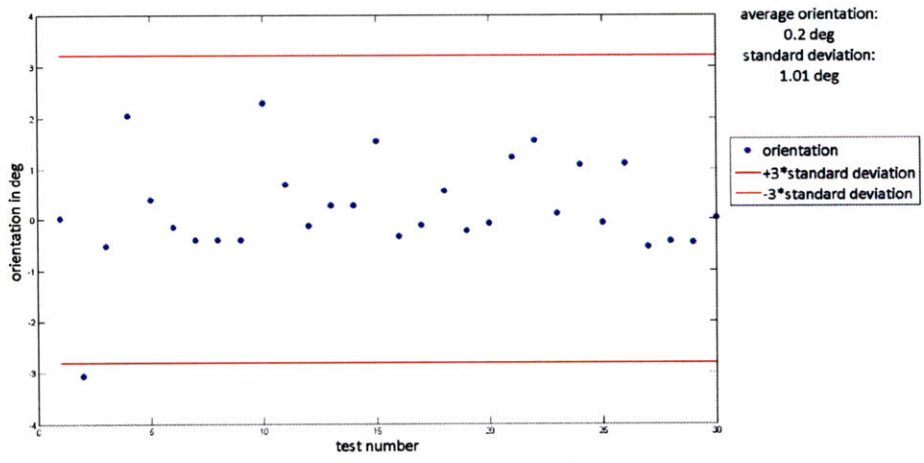

Figure 6.2: Variation of the orientation of the part in the experiment to determine the repeatability of the simple cycle.

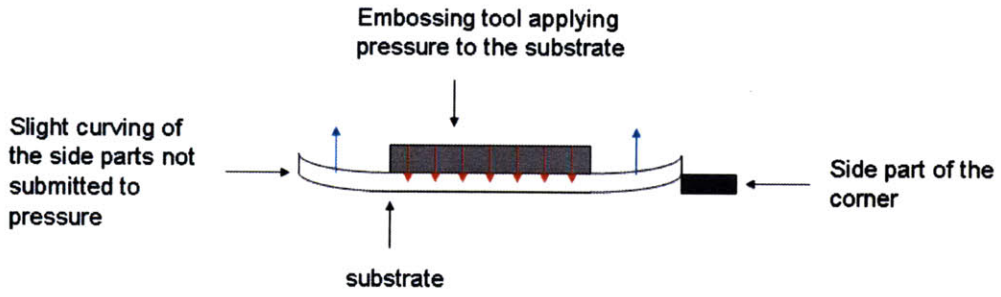

Figure 6.3: Schematic of the warping issue.

To fix this problem, a solution is possible: the master corner in the embossing machine must be higher, so that even if the substrate is curved, its edge will be in contact with the corner.

6.3 Entire cycle

For an entire cycle, the operations are as follows:

- The substrate blank is picked up from the part feeder.
- The blank is positioned and registered in the hot micro embossing machine (HME). The HME cycle is executed.
- The part is positioned and registered in the inspection stage, and inspected. At this point, the inspection stage is the measurement platform described in 4.1. An image of a fiducial (a Swiss flag) is taken.
- The part is placed in the bonding machine.
- A coverplate is picked up out of the coverplate feeder and placed on top of the embossed part in the bonding machine. The bonding cycle is executed.
- The bonded part is picked up from the bonding machine, placed on the inspection stage and inspected a second time.
- The part is picked up from the inspection stage and placed in a Petri dish.

The manipulation has been executed up to the point where the embossed part and the coverplate are precisely aligned in the bonding machine. Unfortunately, the bonding machine was not ready to automatically run its cycle, so the complete automation has not yet been proven to work.

Chapter 7.

Flow of materials and models of the factory

One of the goals of the *μFAC II* is to decrease the Takt time of the assembly to 5 minutes. The optimization of production rate of flow line models is a difficult problem that is very thoroughly explained in [17]. It includes the use of multi-part buffers between each station, and even more importantly, an adaptive control of the manipulation: the states of each buffer and station are constantly sent to the controller in order to dictate the actions of the manipulator.

μFAC II is mostly a deterministic production cell: as a teaching factory, if one of the stations breaks down, the whole factory will be stopped, and someone will come to fix the station. The goal is not to make as many parts as possible in a minimum time while dealing with station errors, but rather to prove that it is possible to do it when n error is present. In this situation, no buffer should be necessary. The role of a buffer is to enable the line to work even if a station is down, by storage of the parts upstream and downstream of this station. In a deterministic production cell, the production rate is the rate of the slowest machine: adding a finite-size buffer after a station to make it work even if the next station is slower is a naïve thought. As soon as the buffer is full (which has to happen eventually for a long run of the line), the situation will be exactly equivalent to a situation without a buffer between both stations. In this case, it would end up being the steady-state behavior defining the production rate, as opposed to the previous transient behaviors.

A simulation of the flow of materials has been conducted. It is assumed for the simulation that the hot-embossing and the bonding steps take 180 seconds, the inspection takes 100 seconds, and each travel and manipulation from one machine to another takes 20 seconds. These times are consistent with the manipulations conducted by the experimenter and the data given in [6]. From

the perspective of the robot, the various machines serve as buffers allowing the robot to manipulate several parts through the stages of the cell simultaneously.

The algorithm to program this simulation is a loop incremented in time each second. Each station, as well as the robot, has a state, corresponding to its action: idle, working, done with its task and so on. For the robot, different states correspond to different travels. No breakdown has been taken into account, since the production cell is supposed to be deterministic. Each change of state is dictated by a logical combination of states: for example, the robot will start to pick a part from the part feeder if and only if the hot embossing machine and the robot are idle. Then, the state of the robot will become "picking a part from the part feeder to the hot embossing machine" for 20 seconds. After this time, the hot embossing machine will become "embossing" and the robot will be idle again. The count of the parts is transmitted from one station to another, making it possible to track each of them through the workflow.

The part flow through the factory where no buffer is used has been simulated and is shown in Figure 7.1. Each color corresponds to an individual part flowing through the cell as a function of time. The hatched blocks in the embossing and the inspection rows indicate that the part is in the station but is idle, waiting to move to the next station or for the robot to finish its current task.

Starting from the bottom row, the robot moves the light-blue (LB) part from the part feeder and places it on the HEM. After embossing completes, the LB part is picked up by the robot and moved to the inspection stage. Immediately thereafter, the next part, yellow (Y), is moved from the part feeder and placed on the hot embossing machine - in this way the production of parts is staggered through the cell. After LB part inspection is complete, the robot moves the part to the bonding machine. Then the robot picks up the coverplate and places it in the bonding machine. After bonding completes, the LB part is in the bonding machine and has to be inspected, while the Y embossed part is in the inspection stage and has to be bonded. Since the robot can handle only one part at a time, no motion is possible: at this point, a buffer, or more precisely a switching platform, is necessary.

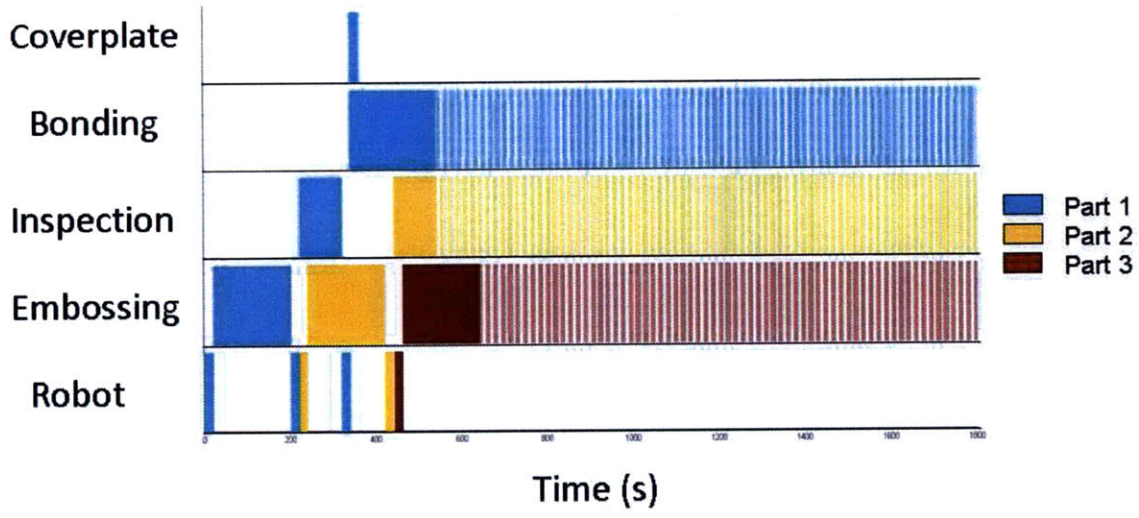

Figure 7.1: Flow of material through a factory where no buffer is used.

The flow of materials is then simulated with one buffer added between the bonding machine and the second inspection. The result is shown in Figure 7.2. The manipulation has been programmed to maximize the occupation of the Inspection Stage, which is the bottleneck of the line. Indeed, since each inspection takes 100s, and two inspections are required, the total time of inspection is 200s (plus the time of travel between two inspections) compared to 180s for the embossing or the bonding steps.

The first steps are similar to the previous simulation for the first two parts, in dark blue (DB) and light blue (LB). But at the point where DB and LB need to switch their positions, the buffer enables the motion and the flow can be established.

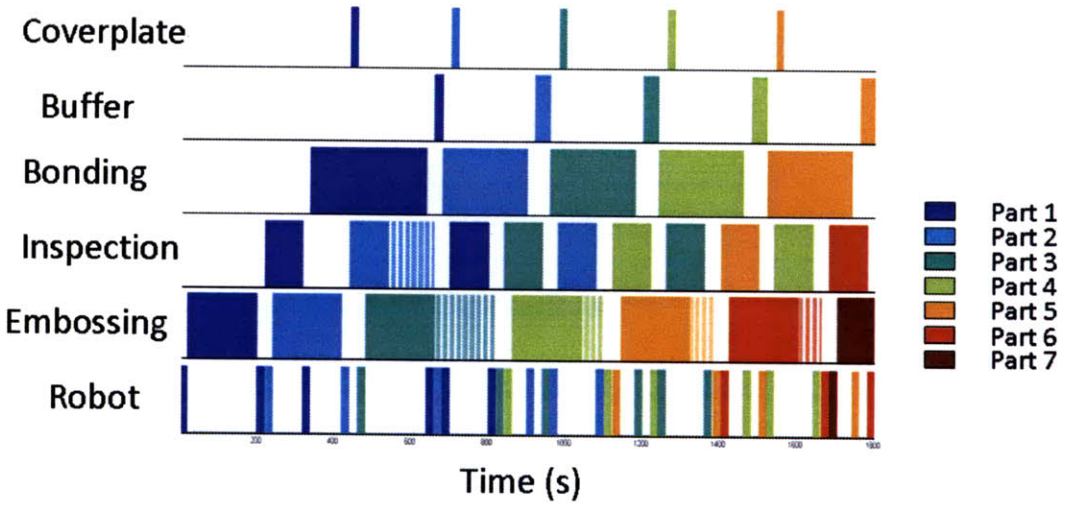

Figure 7.2: Flow of material through a factory where one buffer is used.

Notice that the time between two inspections corresponds exactly to two travels of the robot: the inspection stage couldn't work more. Also notice that .in steady state, a part is finished every 280s. This is the production rate, corresponding to two inspections, plus 4 travels, to and from each inspection.

Starting at the third part (G), the hot embossing machine stays idle for 60s: this corresponds to the difference in production rates between the hot embossing machine and the inspection stage.

To conclude, we observe that only two things could increase the production rate of the line. First, the time of inspection or the time of travel to or from the inspection stage could be shorter. Second, another inspection stage could be introduced to avoid two stays in the same station for each part.

Chapter 8.

Conclusion

Over the course of this project, an automated manipulation for polymer-based microfluidic devices production has been designed, built and tested. An alignment strategy based on compliant kinematic coupling allows an improvement of the position repeatability of the principle manipulator by a factor of 5 for an ideal part, and by more than 2 for a real embossed part. A modeled flow of material in the production cell has been optimized to minimize the Takt time, which had a minimum value of 280s.

A few issues must still be addressed:

- First, the creation of the embossed corner used for the kinematic coupling has to be improved to be robust to warping of the part.
- Secondly, the complete manipulation through the bonding machine has still to be tested once this latter is achieved and functional.
- Third, communication and manipulation with the final inspection stage has not been tested yet, since this station is not ready.
- Finally, a functional test should be included in the production cell and applied to a small fraction of the production. This station is still in the design phase.

However, the design selected and achieved for the manipulation of this production cell has been thought to be modular enough to allow changes and improvements of the existing production design. The addition of the new stations should be easy if their principles are consistent with the current ones.

References

[1] Hardt D.E., Anthony B.W., Tor S.B, "A teaching factory for polymer microfabrication - μFac" to be published, *International Journal of Nanomanufacturing.*

[2]Ames N.M., Srivastava V., Chester S., and Anand L. (2008), "A thermo-mechanically-coupled theory for large deformations of amorphous polymers, Part 1: formulation", *International Journal of Plasticity*, submitted, 2008.

[3]Ames N. M., Srivastava V., Chester S., and Anand L. (2008), "A thermo-mechanically-coupled theory for large deformations of amorphous polymers. Part II: applications", *International Journal of Plasticity*, submitted, 2008.

[4] Dirckx M., "Design of a fast Cycle Hot Micro-Embossing Machine", SM Thesis, Dept. of ME, MIT, May 2005.

[5] Mazzeo A.D., Schrauth A.J., and Hardt D.E. (2008), "Fast Curable Liquid resin Procedure for the Manufacturing of Micro/Nano featured Parts", *ISNM 5*, Singapore, January 2008.

[6] Hale M. (2009) "Development of a Low-Cost rapid-cycle Hot Embossing System for Microscale Parts", MIT MS Thesis, June 2009.

[7]Henann D.L, Srivastava V., Taylor H.K, Hale M., Hardt D.E, and Anand L. (2010), "Zr-based metallic glasses: viable tool materials for production of surface microstructures in amorphous polymers by microhot-embossing", to be published, *J. Micromech. Microeng*, 2010.

[8]Fu G., Tor S.B, Loh N.H and Tay B.Y (2008), "Micro Hot-embossing of 316L Stainless Steel Micro-structures", *5th International Symposium on Nanomanufacturing*, 23-25 January 2008, Singapore

[9] Yeo L.P., Lam Y.C., Chan-Park M.B., Joshi S.C. and Hardt D.E. (2005), "Demolding of high aspect ratio polymeric micro-patterning", *International Journal of Nanoscience*, 4(4), 543.

[10]Xu Z.,Li S.G, Yoon S.F, Youcef-Toumi K., Burns D.J, Shilpiekandula V., Taylor H.K, and Boning D.S (2008) "Complete surface distinguishing and overlapping technology for three-dimensional image processing of micro devices", *5th ISNM*, Singapore, January 2008.

[11]Taylor H.K, and Bonding D. S. (2008), "An integrated crack-opening method for determining the work of fracture of bonded polymer interfaces", *Micro Total Analysis Systems*, October 2008.

[12]Shilpiekandula V., Burns D.J, Li S.G, Xu Z., Taylor H.K, Yoon S.F, Reading I. (2008) "Fusion of metrology data for large-scale high-volume manufacturing of polymer-based microfluidic devices",*5th ISNM*, Singapore, January 2008.

[13] Wang Q, and Hardt, D.E. (2006), "Processing Window Identification and Process Variability Study of Micro Embossing", Proc., *1st International Conference on Micro-manufacturing, UIUC*, IL, Sept 2006.

[14] Taylor H.Kand BoningD.S. (2008), "Diffraction-based approaches to the in-situ measurement of dimensional variations in components produced by thermoplastic micro- and nano-embossing," presented at *5th International Symposium on Nanomanufacturing*, Singapore, Jan. 2008.

[15] Mazzeo A. (2009), "Centrifugal Casting and Fast Curing of Polydimethylsiloxane (PDMS) for the Manufacture of Micro and Nano Featured Components", MIT PhD Thesis, May 2009.

[16] Anthony B.W., Hardt D.E.,Hale M, Zarrouati N (2010), "A Research Factory for Polymer Microdevices: muFac", *Journal of Micro/Nanolithography, MEMS, and MOEMS.*

[17] Dallery Y, Gershwin S.B (1992) "Manufacturing flow line systems: a review of models and analytical results", *Queueing Systems* 12 (1992) 3-94

[18] SCARA ROBOT G10 / G20 series MANIPULATOR MANUAL Rev 6.

[19] Robot Controller RC170/RC180 Rev 7.

[20]Tichem M., Lang L., Karpuschewski B., "A classification scheme for quantitative analysis of micro-grip principles"*Assembly Automation;* 2004; 24, 1;

[21]Ansel Y., Schmitz F., Kunz S., Gruber H.Pand Popovic G., "Development of tools for handlingand assembling microcomponents", *J. Micromech. Microeng*, 12(2002) 430–437

[22]Pellerin C.,"Vacuum basics", *The Industrial Robot.* 1995. Vol. 22, Iss. 4; pg. 27

[23] Slocum A.H, "Precision Machine Design", Dearborn: Society of Manufacturing Engineers, 1995.

[24]. Lozano-Pérez T. (1985), "Compliance in Robot Manipulation", *Artificial Intelligence,*25(1):5-12 (1985)

[25] Brown R.G and Hwang P.Y.C (1992), "Introduction to random signals and applied Kalman filtering", Chapter 1. Wiley

[26] Suction Cup Selection Guide. Anver Corporation

Appendix: Image processing algorithm to detect the position

An image processing algorithm has been developed to detect with accuracy the position of a cross-feature in an image.

Two solutions were considered, studied separately then combined:

- The first one is based on binary morphological operations: it uses the fact that the feature to detect is known to be a cross, oriented to be roughly aligned with the vertical and horizontal directions. It detects separately the horizontal and the vertical lines, then compute their intersection and deduce the position and the orientation of the feature.
- The second one is based on the correlation of the image with the detail that is looked for in it, a strategy called Template Matching. It is really efficient when the template and the image are oriented in the same way, but the rotation of the image makes the problem tricky. The find the exact orientation of the image, a dichotomy algorithm is used, based on the minimization of the peak corresponding to the overlap of the template and the image.

We will present both solutions with their strengths and weaknesses, then the combination of both in the final algorithm, along with its characteristic efficiency.

Solution based on binary morphological operations:

Following is the summary of the steps used for this solution applied to an image such as in Figure 8.3.a:

- Step 1: The original image in color is converted in black and white (Figure 8.3.b)

- Step 2: The image is convoluted with a vertical kernel (Figure 8.3.c)
- Step 3: The image is made binary: the pixels whose value are more a certain threshold are set to 1, the rest is 0 (Figure 8.3.d)
- Step 4: Binary morphological operations are conducted to smooth the overall feature by connecting the representative individual features and erase the noise (Figure 8.3.e)
- Step 5: Each individual feature (a set of connate pixels) is registered and a line is fitted through each of these components (Figure 8.3.f)
- Step 6: The most representative line is chosen based on the weight and the orientation. The area of the image where this line stands is selected (Figure 8.3.g).
- Step 7: Another convolution of this area and a more consistent vertical kernel is conducted (Figure 8.3.h)
- Step 8: The new image is made binary (Figure 8.3.i)
- Step 9: Morphological operations are conducted (Figure 8.3.j)
- Step 10: Line are fitted though each connate component as in Step 5 (Figure 8.3.k)
- Step 11: The most representative line is selected (Figure 8.3.l)
- Steps 12 to 21: operations equivalent to Steps 2 to 11 are processed to fit a horizontal line.
- Step 22: The intersection of both lines is computed, as well as their orientation.

To analyze this algorithm, a set of images of a part always in the same position has been taken: only the light and the shadows vary. Then the positions and orientations of the cross are computed by the algorithm, from which the sensitivity of the algorithm can be deduced. The positions are plotted in Figure 8.1and the variation of the orientation in Figure 8.2.

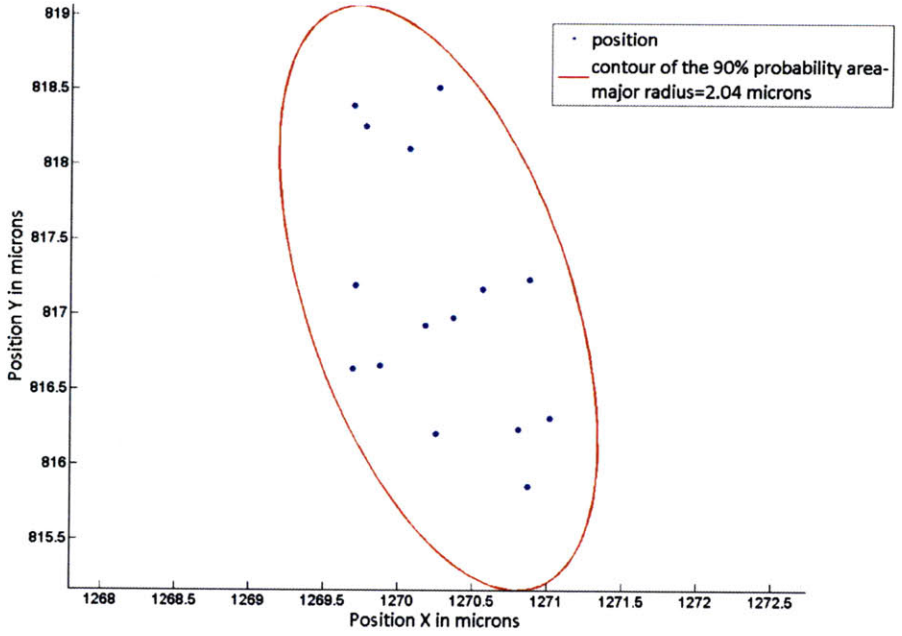

Figure 8.1: Positions of the part in the analysis of the Algorithm based on Binary Morphological operations

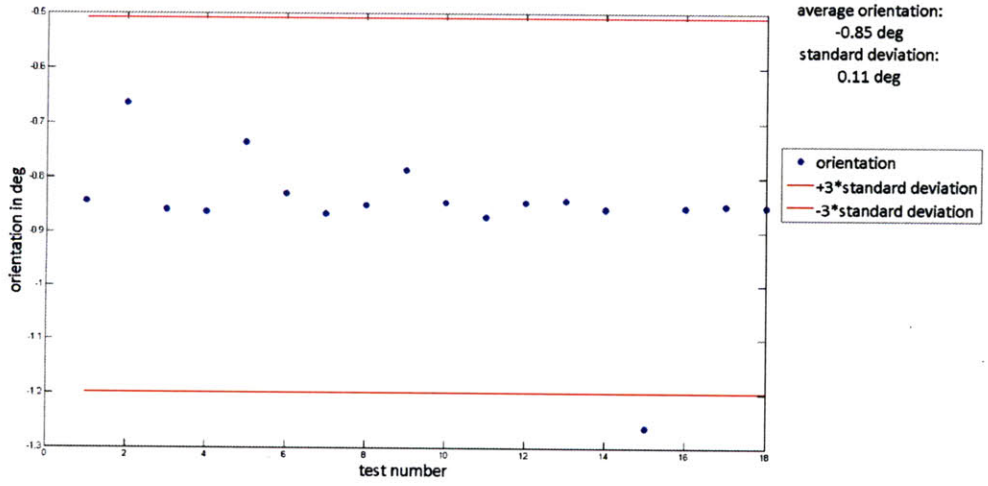

Figure 8.2: Variation of the orientation of the part in the analysis of the Algorithm based on Binary Morphological operations

This solution is really efficient and fast for images where the arms of the cross are roughly horizontal and vertical. However, as soon as the orientation becomes larger than 15°, it is not robust enough. Moreover, the accuracy of this solution depends a lot on the width of the cross: for large details, the line fitting can vary.

a)

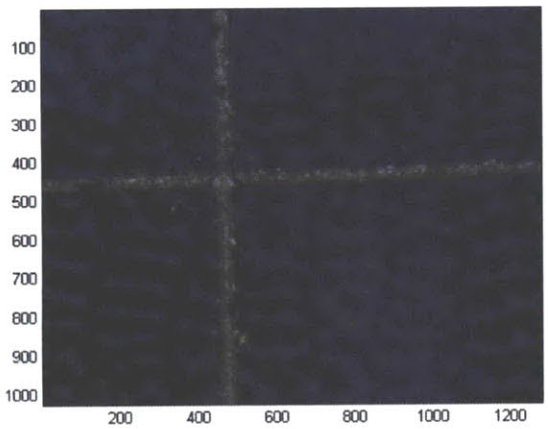
100
200
300
400
500
600
700
800
900
1000
200
400
600
800
1000
1200

b)

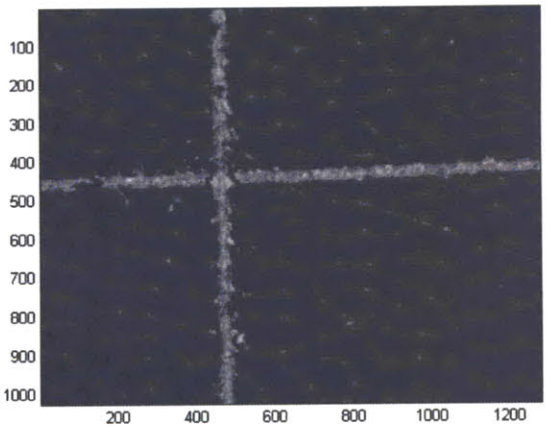
100
200
300
400
500
600
700
800
900
1000
200
400
600
800
1000
1200

c)

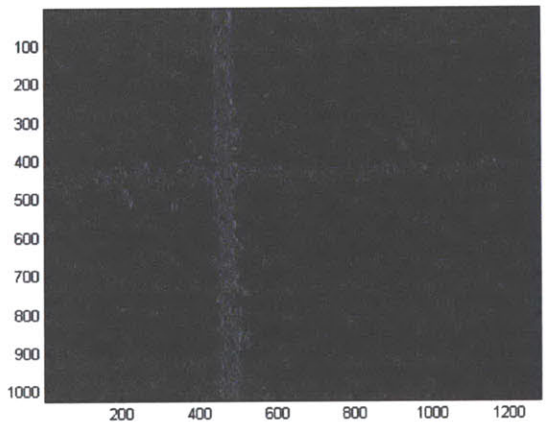
100
200
300
400
500
600
700
800
900
1000
200
400
600
800
1000
1200

d)

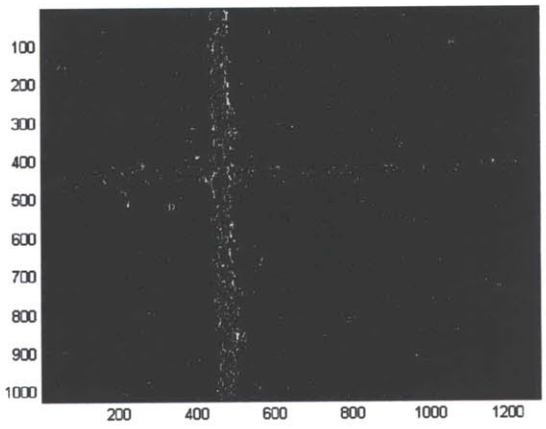
100
200
300
400
500
600
700
800
900
1000
200
400
600
800
1000
1200

e)

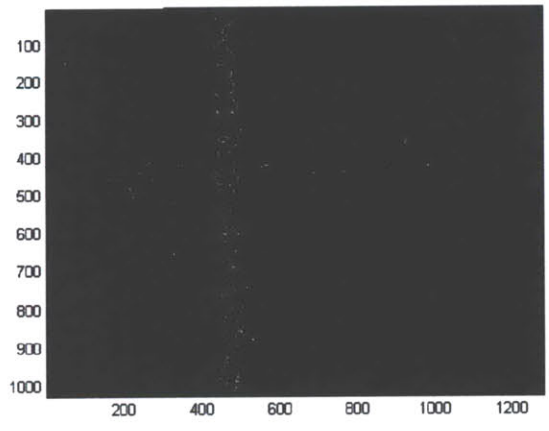
100
200
300
400
500
600
700
800
900
1000
200
400
600
800
1000
1200

f)

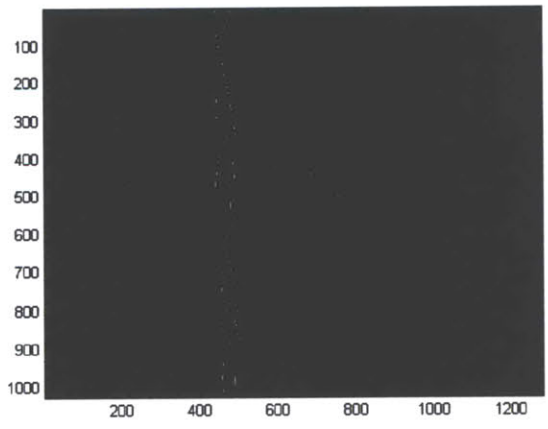
100
200
300
400
500
600
700
800
900
1000
200
400
600
800
1000
1200

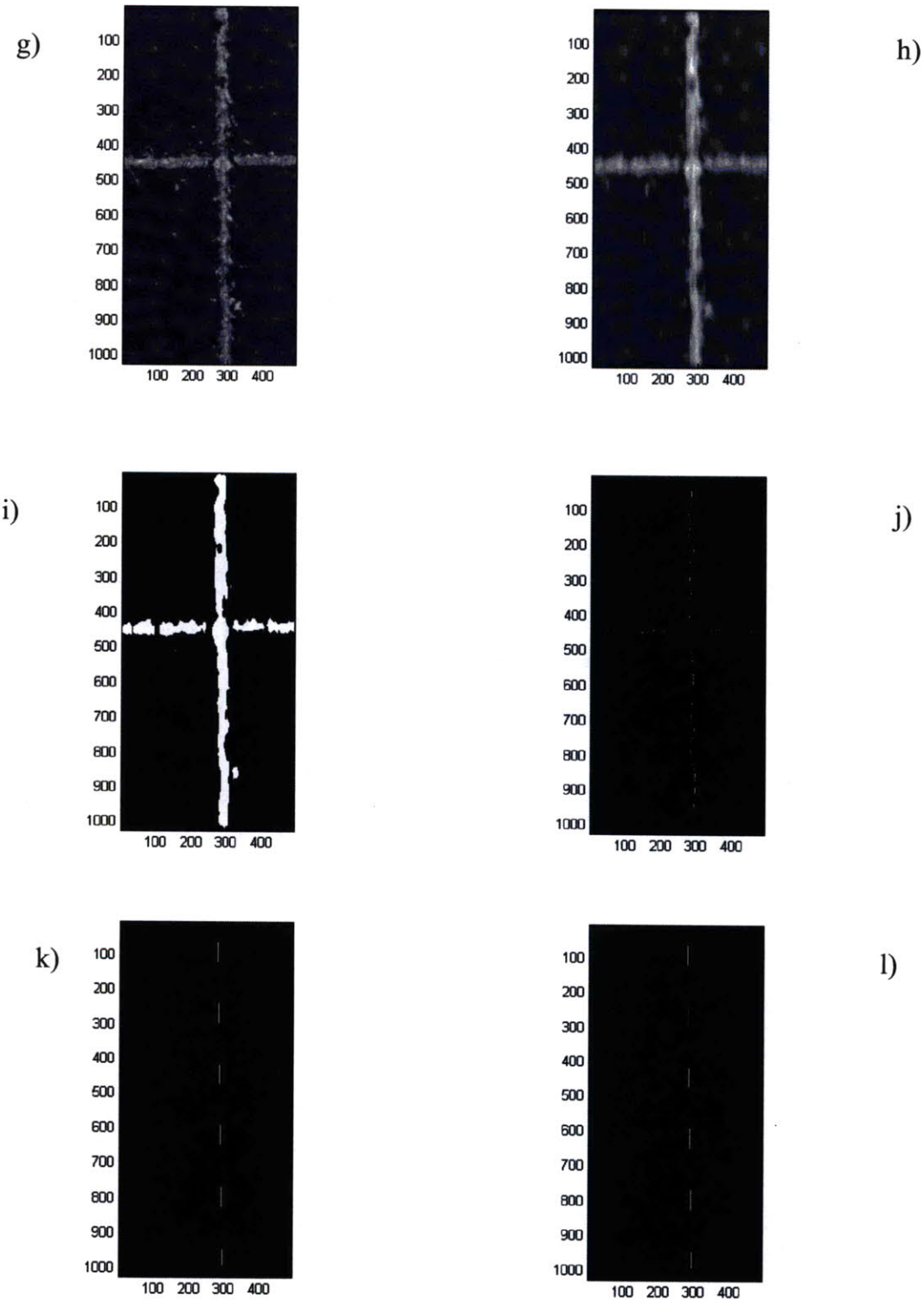

Figure 8.3: Image processing steps and binary morphological operations.

Solution based on Template Matching:

The Template Matching concept is theoretically simple. It consists of 3 steps:

- Step 0: A detail is chosen on the original image to be the template. Of course, we know exactly where this template is in the original image, but the goal is to use the same template for a whole set of images, and to find its position and orientation on each of them.
- Step 1: The image in colors is converted into black and white.
- Step 2: A convolution of the image with the template is processed.
- Step 3: The peak corresponding to the region where the template and the image overlap is selected. The position of the peak is computed, as well as its width.

The tricky part is that this strategy works really well for one dimension signals such as sound, but for images which are two dimensional objects, the template and the image can be not oriented in the same way: even is the exact same template is present in the image, the convolution won't recognize it. This is why an algorithm based on the minimization of the width of the peak has been developed. Indeed, a perfect match would correspond to a thin and intensive peak, as opposed to a wide and blurry peak for an approximate match. This algorithm proceeds by dichotomy. The basic operation consists in the following, using one image, one template and two different angles as the inputs:

- Step 1: the Template Matching operation is conducted on the image and the template rotated by θ_1. The width of the peak W1 is computed.
- Step 2: the Template Matching operation is conducted on the image and the template rotated by θ_2.The width of the peak W2 is computed.
- Step 3: The angle θ_{min} corresponding to the minimum width is selected. The outputs are two angles: θ_{min} and $(\theta_1+\theta_2)/2$. If both peaks have the same width, the smallest angle is slightly increased and the largest is decreased to reduce the interval and allow the algorithm to converge.

The whole algorithm is recursive: first, the inputs are ±15°, and then the basic operation will go on until the difference between the angles is small enough and the positions of the corresponding peaks are equal.

The same test has been conducted for the analysis of the Template Matching algorithm than for the previous algorithm: the new algorithm is now applied to the same set of images than before, and the positions and orientations are computed (Figure 8.4 and Figure 8.5).

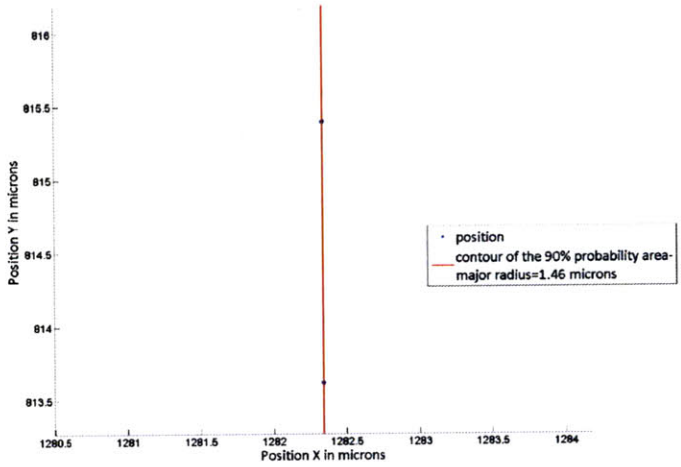

Figure 8.4: Positions of the part in the analysis of the Algorithm based on Template Matching

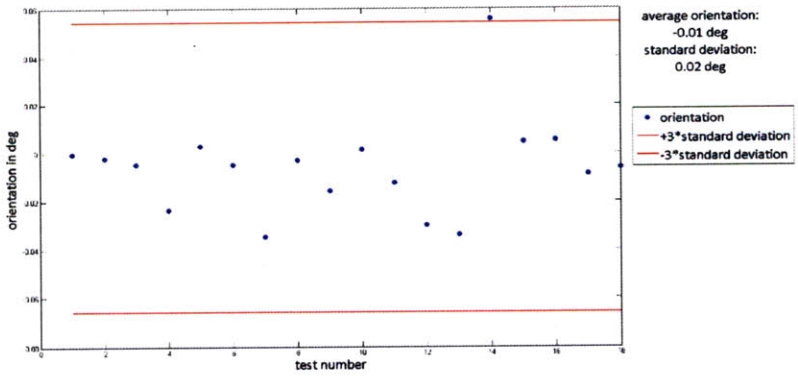

Figure 8.5: Variation of the orientation of the part in the analysis of the Algorithm based on Template Matching

Notice there are only two positions detected, which correspond to the pixel where the best match has been found. For that algorithm, the definition of the repeatability that has been used from now doesn't stand: since the algorithm gives the position with an uncertainty of the size of a pixel, that size should be defined as the repeatability. That value, 1.75 microns, is better than the repeatability of the previous algorithm. The repeatability of the orientation is 0.02 deg, which is also better than for the previous algorithm.

This algorithm is accurate for the position, but it really slow: the convolution of a matrix of 1280 by 1024 pixels by a Template of 300 by 300 pixels can take 3 minutes. Multiply this by the number of iterations necessary to solve the recursive algorithm, and the process of one image can take up to one hour. This is why it is necessary to reduce the size of the image without reducing the accuracy of the result. The solution is to combine both of the strategies previously presented.

Combination of the solutions:

The final algorithm uses both solutions to improve their speed, robustness and accuracy.

First, the solution based on binary morphological operations is processed. The outputs are the position P_1 where the center of the cross is supposed to be, and its orientation θ.

Then, an area of the image centered on P_1 and slightly larger than the template is selected.

The Template Matching algorithm is applied to this area: the input angles are $\theta \pm 5°$. Each of the convolutions is faster than previously, and the number of iterations is smaller. The result is an angle θ_f and a position P_2.

Finally, the positions $P_1$and P_2 are combined to find the real position of the template in the image. The final orientation is θ_f.

For this solution, the repeatability in position and orientation is the same as for the Template Matching algorithm: 1.75 microns for the position, 0.02 deg for the orientation. The strength of this algorithm is to combine the speed of the algorithm based on binary morphological operations and the accuracy of the algorithm based on Template Matching. The time necessary to detect the positions of a detail on one image is about 10 minutes.